Limited expression of the Paleoproterozoic Oklo natural nuclear reactor phenomenon in the aftermath of a widespread deoxygenation event ~2.11-2.06 billion years ago

Frantz Ossa Ossa[a,b]*, Andrey Bekker[c,b], Axel Hofmann[b], Simon W. Poulton[d], Christophe Ballouard[e], Ronny Schoenberg[a,b]

[a]Department of Geosciences, University of Tuebingen, 72074 Tuebingen, Germany

[b]Department of Geology, University of Johannesburg, 2092 Johannesburg, South Africa

[c]Department of Earth and Planetary Sciences, University of California, Riverside, CA 9252, USA

[d]School of Earth and Environment, University of Leeds, Leeds LS2 9JT, UK

[e]GeoRessources, University of Lorraine, CNRS, 54000 Nancy, France

*Correspondence to: frantz.ossaossa@gmail.com.

Abstract

The only known case of natural fission reactors is hosted by high-grade uranium (U) deposits at Oklo-Okelobondo and Bangombé in sandstones of the ~2.1 Ga Francevillian Group, Gabon. However, the geochemical influence of the depositional environment on this unique natural nuclear phenomenon has not been clearly established. Localized, unusually high vanadium (V) enrichments are thought to have prevented such natural nuclear fission reactors from occurring in other Francevillian U deposits (e.g., Mounana, Boyindzi, and Mikouloungou). However, while U-bearing detrital monazite derived from Archean rocks surrounding the Francevillian basin is viewed as the main source of U, the source of V remains poorly constrained. Here, we combine petrographic and whole-rock geochemical data for the Francevillian Group sedimentary rocks, coupled with previously documented geochemical data for the Archean basement. These data suggest that, although ultramafic to mafic igneous rocks of the Mesoarchean Bélinga Group, and to some extent Archean granitoids, were likely important sources of V to the Francevillian U deposits, they were not the only source of the

abnormally high V concentrations in the U deposits that did not produce natural nuclear reactors. Instead, hydrocarbon migration from V-rich black shales of the Upper Francevillian Group, deposited during widespread and protracted deoxygenation of the Paleoproterozoic ocean at the end of the Lomagundi Carbon Isotope Excursion (LE) at ~2.11-2.06 Ga, resulted in a redox front that precipitated the U deposits. These migrated V-rich hydrocarbons likely account for the high V concentrations, which ultimately prevented natural fission reactions from occurring in these U deposits. Similarities with other pyrobitumen-bearing Paleoproterozoic U deposits worldwide suggest that organic-rich source rocks, which deposited in open-marine settings under widespread hyper-euxinic conditions in the aftermath of the LE, played a key role in preventing the Oklo natural nuclear reactor phenomenon from reaching a larger extent.

Keywords: Uranium deposits, natural nuclear reactors, Oklo, Francevillian, vanadium, deoxygenated ocean

1. Introduction

Five economically significant, redox-controlled, sandstone-hosted U deposits have been identified in the ~2.1 Ga Paleoproterozoic Francevillian Group: the Mounana, Boyindzi, Oklo-Okelobondo, Mikouloungou and Bangombé deposits (e.g., Bonhomme et al., 1982; Bros et al., 1992; Horie et al., 2005; Gauthier-Lafaye and Weber, 1989, 2003; Guauthier-Lafaye, 1986, 2006). The dominant U-bearing minerals in these U deposits mostly comprise authigenic uraninite and coffinite (Cuney, 2010; Gauthier-Lafaye, 2006; Guauthier-Lafaye, 1986; Gauthier-Lafaye and Weber, 1989). Detrital minerals, such as monazite derived from weathering of Mesoarchean granitoids surrounding the basin, are generally assumed to be the

main source of U in the Francevillian Group (Cuney and Mathieu, 2000; Gauthier-Lafaye, 1986; Gauthier-Lafaye and Weber, 1989, 2003; Mathieu et al., 2000, 2001; Ossa Ossa et al., 2020). Hydrothermal alteration (by oxidized fluids) of these U-bearing minerals in sandstone and conglomerate units of the lower Francevillian Group, and possibly in granitoids of the Mesoarchean basement, mobilized a significant amount of U along regional faults (Mathieu et al., 2000, 2001; Ossa Ossa et al., 2014). The formation of high-grade U ores occurred when these oxidized U-bearing fluids mixed with reduced fluids migrated from black shales of the upper Francevillian Group (Cuney, 2010; Cuney and Mathieu, 2000; Gauthier-Lafaye, 1986, 2006; Gauthier-Lafaye and Weber, 1989; Mathieu et al., 2000, 2001; Ossa Ossa et al., 2014).

A key characteristic of the Francevillian U deposits is the presence of natural nuclear reactors in the Oklo-Okelobondo and Bangombé deposits. Fission reaction of ^{235}U occurred spontaneously in these natural reactors at ~1950 Ga (Gauthier-Lafaye, 2002, 2006; Gauthier-Lafaye et al., 1996; Naudet, 1991; Neuilly et al., 1972). For natural nuclear reactors to occur, three critical conditions, established for pressurized water reactors (PWR), must be met (e.g., Naudet, 1991), including: (1) a high U concentration, (2) the presence of water or organic carbon to slow down fast neutrons produced by fission reactions, and (3) a $^{235}U/^{238}U$ ratio higher than 0.03 (Bentridi et al., 2011; Naudet, 1991). Francevillian U deposits are characterized by high UO_2 contents of up to 15%, and U precipitation took place in porous sandstones where primary and secondary pores were filled by migrated, reduced waters and hydrocarbons in association with the ~2.2-2.0 Ga Eburnean Orogeny, when the Congo and São Francisco cratons collided forming the core of the Nuna/Columbia supercontinent (Bankole et al., 2020; Ossa Ossa et al., 2020). Natural nuclear reactors occurred later when Earth's decreasing $^{235}U/^{238}U$ ratio was approximately 0.0368, just above the threshold ratio required for fission reactions (e.g., Bentridi et al., 2011; Gauthier-Lafaye, 2002, 2006; Naudet, 1991).

Similar to PWR nuclear plants, these conditions allowed natural fission reactions to be sustained in the lower Francevillian Group sedimentary strata (Bentridi et al., 2011; Gauthier-Lafaye, 2002, 2006; Naudet, 1991). However, it is still unclear why natural nuclear reactors occurred only in association with the U deposits at Oklo-Okelobondo and Bangombé, with no such phenomenon documented in other U deposits at Mounana, Bouyindzi and Mikouloungou, although the three critical conditions described above were met at all these locations (Gauthier-Lafaye, 2002, 2006; Gauthier-Lafaye et al., 1996; Gauthier-Lafaye and Weber, 1989; Naudet, 1991). The same applies to U deposits of broadly similar age formed in other locations around the world, such as the Onega basin in Russia, where metasomatically modified U deposits are stratigraphically restricted to the boundary between organic-rich sediments of the Zaonega Formation and oxidized carbonates and red beds of the Tulomozero Formation (e.g., Cuney, 2010; Boitsov, 1995; Boitsov and Nikolsky, 1997).

Besides the three critical conditions described above, the concentration of 'neutron poisons', with their capability to absorb fast neutrons, may prevent fast neutrons from exponentially accelerating the fission rate. In natural environments, rare earth elements (REEs), boron (B) and vanadium (V) represent the most important 'neutron poisons'. Studies of the Francevillian U deposits have shown that the REE and B contents are similar and low in all deposits (Gauthier-Lafaye, 2002, 2006; Gauthier-Lafaye and Weber, 2003; Naudet, 1991). By contrast, the V contents are very high, up to 1.5 wt.%, in the Mounana, Boyindzi and Mikouloungou U deposits, where natural nuclear reactors did not occur (Gauthier-Lafaye, 2002, 2006; Gauthier-Lafaye et al., 1996; Gauthier-Lafaye and Weber, 2003; Naudet, 1991; Weber, 1968). On the other hand, V contents are much lower in the Oklo-Okelobondo and Bangombé U deposits that are associated with natural nuclear reactors (Gauthier-Lafaye, 2002, 2006; Gauthier-Lafaye and Weber, 2003; Naudet, 1991). Vanadium thus appears to have

played a first-order control on the extent of natural fission reactions in the U deposits of the Francevillian basin (Naudet, 1991).

This study aims to provide new insight into the potential sources of V that restricted the natural nuclear reactor phenomenon to the Oklo-Okelobondo and Bangombé U deposits. In addition, we investigate implications for Paleoproterozoic environmental conditions during this unique phenomenon.

2. Geological setting of Francevillian U deposits

The Francevillian basin covers an area of about 44,000 km^2 in southeastern Gabon, and is subdivided into four sub-basins, including Booué (Plateau des Abeilles), Lastoursville, Franceville and Okondja (Fig. 1A). The lithostratigraphy is characterized by five sedimentary formations, from Francevillian A (FA) at the bottom, to FE at the top (Fig. 1B), with deposition occurring during the Lomagundi carbon isotope excursion (Bonhomme et al., 1982; Bouton et al., 2009; Bros et al., 1992; Gauthier-Lafaye and Weber, 1989, 2003; Horie et al., 2005; Ossa Ossa et al., 2013, 2018; Préat et al., 2011; Thiéblemont et al., 2009; Weber, 1968). The Lomagundi carbon isotope excursion (LE; ~2.22-2.06 Ga) is Earth's most pronounced and long-lived carbon isotope excursion, representing a period of high organic carbon burial and enhanced O_2 production in the atmosphere-ocean system (Karhu and Holland, 1996; Bekker, 2014) that was the tipping point for permanent atmospheric oxygenation (Poulton et al., 2021). The FA Formation is characterized by conglomerate, sandstone and shale deposited in fluvial settings in its lower part, and tidally influenced fluvio-deltaic environments in the upper part (Gauthier-Lafaye, 1986; Gauthier-Lafaye and Weber, 1989, 2003; Ossa Ossa, 2010; Ossa Ossa et al., 2014; Weber, 1968). Fluctuations between inner and outer shelf marine environments characterized deposition of interbedded black shale, siltstone, sandstone and carbonate in the

126 FB Formation. A peritidal-sabkha carbonate platform with stromatolitic buildups and open-
127 shelf shale deposits characterized the FC Formation (Gauthier-Lafaye and Weber, 1989, 2003;
128 Ossa Ossa et al., 2018; Préat et al., 2011; Weber, 1968). For the FD and FE formations, marine
129 black shales interbedded with sandstones dominate, with episodes of pronounced submarine
130 and subaerial volcanism (Gauthier-Lafaye and Weber, 1989, 2003; Préat et al., 2011; Weber,
131 1968).

132 All U ore deposits in the Francevillian basin are hosted by the FA Formation sandstones
133 (Gauthier-Lafaye, 1986; Gauthier-Lafaye and Weber, 1989, 2003; Mathieu et al., 2000) (Figs.
134 1B, 2). Three main types of circulating fluids are considered to have caused U mineralization
135 in FA sandstones (Gauthier-Lafaye, 1986; Gauthier-Lafaye and Weber, 1989, 2003; Mathieu
136 et al., 2000; Openshaw et al., 1978) (Fig. 2). These include oxidized and low-salinity meteoric
137 fluids that descended into the basin along regional faults. These fluids experienced heating in
138 the Archean basement to temperatures averaging 240 ± 30°C (Ossa Ossa et al., 2014) before
139 ascending to the overlying FA Formation with significant amounts of dissolved U. Highly
140 saline diagenetic brines in the FA Formation sandstone and conglomerate further drove
141 leaching of U-bearing detrital minerals at temperatures up to ~150°C (Mathieu et al., 2000;
142 Openshaw et al., 1978). These saline diagenetic brines mixed with ascending hot and low-
143 salinity fluids to form oxidized fluids with high dissolved U contents (Mathieu et al., 2000;
144 Openshaw et al., 1978). The currently accepted view infers that organic-rich fluids and
145 hydrocarbons were generated from black shales of the FB Formation and migrated to sandstone
146 reservoirs within the FA Formation, where structural traps were formed during foreland basin
147 development (Fig. 2; Lecomte et al., 2020; Mathieu et al., 2000; Gauthier-Lafaye and Weber,
148 1989, 2003; Openshaw et al., 1978; Weber et al., 2016). Finally, mixing of U-rich, oxidized
149 and mineralizing fluids and hydrocarbons in structural traps caused U precipitation and

150 formation of high-grade U-ore deposits (Fig. 2; Gauthier-Lafaye, 1986; Gauthier-Lafaye and
151 Weber, 1989; Mathieu et al., 2000; Openshaw et al., 1978).

152

153 **3. Analytical methods**

154 3.1. Petrography

155 Petrographic analysis was performed on polished thin sections using an OLYMPUS
156 BX51 polarizing optical microscope equipped with an OLYMPUS DP72 camera. Carbon-
157 coated polished thin sections were analyzed using a TESCAN VEGA 3 scanning electron
158 microscope (SEM) at Spectrum, University of Johannesburg. The SEM is equipped with an
159 electron back-scattering detector and an energy dispersive spectrometer (EDS). The operating
160 conditions were 20 kV accelerating voltage for both imaging and elemental analysis. The goal
161 of the petrographic analysis was to characterize detrital mineral assemblages, their alteration
162 products, and distribution of U and V in these minerals in the FA Formation structural traps
163 where natural nuclear reactors are present and absent (Fig. 3). Since a more comprehensive
164 regional characterization of mineral phases in the Francevillian Group
165 sandstones/conglomerates and black shales has already been presented in earlier publications
166 (e.g., Ossa Ossa, 2010; Ossa Ossa et al., 2013, 2014, 2020), only the most representative
167 characteristics are discussed here. Further detailed petrographic descriptions of the FA
168 Formation sandstones and conglomerates can be found in published literature (e.g., Bankole et
169 al., 2015, 2016; Gauthier-Lafaye, 1986; Gauthier-Lafaye and Weber, 1989; Jensen and Ewing,
170 2001; Mathieu et al., 2001; Mossman et al., 1993).

171

172 3.2. Major and trace element analyses

Analysis of powdered shale samples for major element concentrations (Table 1) was carried out on fusion beads, using a PANalytical MagiX Pro PW2540 spectrometer at the University of Johannesburg and a wavelength dispersive Bruker AXS Pioneer S4 (Rh-tube at 4 kW) spectrometer at the University of Tuebingen. Accuracy was checked with certified reference materials and was better than 1% (1SD). Elemental concentrations are reported in wt.% with a detection limit of 0.004 wt.%. Al, Fe, Mn and S concentrations for some samples in Table 1 were previously presented in Ossa Ossa et al. (2018), while other data are new measurements produced in this study (see reference to samples analyzed in Ossa Ossa et al. (2018) in Table 1).

Trace element concentrations (Table 1) were measured at the Isotope Geochemistry Laboratory, University of Tuebingen according to the analytical procedure described in detail in previous studies (Albut et al., 2018; Babechuk et al., 2010, 2015). All V, Cr, U, Mo and Ni concentrations presented in Table 1 are newly acquired data from this study. Around 30 mg of ashed, powdered samples (heated to 600°C for 12 h) were dissolved using a mix of concentrated and distilled HF (2 mL) and HNO_3 (0.3 mL) in screw-top 15 mL Savillex© PFA beakers at 120°C for 4 days. After evaporation at 80°C, samples were taken up in 1.5 mL 6 M HCl and re-dissolved in closed beakers at 130°C for 1 day. The samples were evaporated to dryness at 90°C and reacted twice with 0.3 mL aliquots of concentrated HNO_3, with evaporation at 90°C between addition of these aliquots, to remove excess F and Cl. An aliquot of 5 M HNO_3 (1 mL) was added to the sample residues and heated at 80°C for ~1 h to re-dissolve the samples. Analyses were performed with an iCap-Qc ICP-MS coupled to an ESI SC-2 DX auto-sampler with an ESI Fast uptake system equipped with a 4 mL sample loop. For analysis, solution samples in 1 mL 5 M HNO_3 were diluted twice; first in MQ water (dilution factor 1000) and second in an internal standard solution made of 0.3 M HNO_3 (dilution factor 10,000), containing a spike mixture of ^{6}Li (~3 ppb), In (~1 ppb), Re (~1 ppb) and Bi (~1 ppb).

198 Analytical accuracy, estimated relative to 1 RSD from the mean, varied between 3 and 15%,
199 and was monitored by repeated measurements of reference materials OU-6, QS-1, W-2a and
200 AGV-2.

201

202 **4. Results**

203 4.1. Petrographic description of the FA Formation samples

204 Petrographic investigation shows that mineral assemblages in the Francevillian Group
205 sandstones and conglomerates are indistinguishable between areas with and without natural
206 nuclear reactors. All the FA Formation structural traps show an abundance of heavy detrital
207 minerals mainly represented by monazite (Mnz), zircon (Zrn), chloritized Fe-rich silicate
208 grains, and partially altered rutile and titanomagnetite (Figs. 3A, 3B, 3C, 3D). At U-mineralized
209 sites, U-rich phases (e.g., zircon, galena, huttonite, Fe-chlorite, oxides) commonly contain a
210 significant amount of REEs and metalloids, such as arsenic (As) and tantalum (Ta) (Figs. 3E1,
211 E3, E4, 3F1, F3, F4). U-bearing, monazite-group minerals enriched in REEs have been
212 previously described in detail from these sites (Cuney and Mathieu, 2000; Mathieu et al., 2001;
213 Ossa Ossa, 2010; Ossa Ossa et al., 2014, 2020). Vanadium, in the form of oxide minerals, is
214 associated with Ba, Pb, U and Ti, and is also found in clay minerals (Fe-chlorite) (Figs. 3C,
215 3D, 3E, 3F). Vanadium is present in all the FA Formation structural traps, but is more highly
216 enriched in mineralized areas without natural nuclear reactors, as illustrated by authigenic Fe-
217 chlorite (Figs. 3E2, 3F2).

218

219 4.2. Variations in V and U concentrations throughout the Francevillian Group

In the FA Formation, with the exception of U-mineralized structural traps, concentrations of V (4-56 µg/g) and U (0.7-2.5 µg/g), along with other redox-sensitive elements, are not particularly high relative to average upper continental crust (UCC; Fig. 4; Table 1; i.e., V_{UCC} = ~97 µg/g and U_{UCC} = ~2.7 µg/g). The same applies to the FB Formation. Although Mo concentrations (0.2-16.7 µg/g), in association with the manganese-rich stratigraphic interval in the Upper FB_1 Member, are slightly above average UCC value (Mo_{UCC} = 1.1 µg/g), V (11-101 µg/g) and U (0.8-3.5 µg/g) concentrations are similar to, or below, average UCC values (Fig. 4; Table 1). By contrast, concentrations of these elements are much higher in the FC and FD formations, i.e., V (75-588 µg/g), U (1.9-11 µg/g), Mo (0.2-27 µg/g), compared to the rest of the Francevillian Group (besides U-mineralized structural traps), and well above average UCC (Fig. 4; Table 1).

5. Discussion

5.1. Identification of potential sources for V addition to the Francevillian sediments

In modern marine and terrestrial environments, continental runoff following physical and chemical weathering represents the main input for V and other redox-sensitive trace metals (e.g., U, Mo, Cr), with much smaller contributions from submarine volcanism and aerosols (Algeo and Maynard, 2008; Breit and Wanty, 1991; Huang et al., 2015; Schlesinger et al., 2017). However, it has been proposed that due to the large seawater dissolved V reservoir, accumulations of V in sediments are much more pronounced in marine settings compared to terrestrial environments, regardless of whether the sediment provenance is characterized by V-rich lithologies such as mafic and ultramafic rocks (Breit and Wanty, 1991).

Redox processes, adsorption onto mineral phases, and organic complexation are regarded as the most important output channels for dissolved V from seawater (Breit and

Wanty, 1991; Huang et al., 2015; Schlesinger et al., 2017). Vanadium has three main oxidation states: V (vanadate, poorly reactive), IV (vanadyl, highly reactive), and III (e.g., $V(OH)_3$, highly reactive). Vanadate is soluble under oxic seawater conditions and is reduced to insoluble vanadyl or V(III) under suboxic to anoxic conditions. Therefore, vanadium drawdown efficiency and sedimentary enrichment is much higher for sediments deposited under reducing compared to oxidizing conditions (Algeo and Maynard, 2008; Bennet and Canfield, 2020; Breit and Wanty, 1991; Huang et al., 2015; Lewan, 1984; Schlesinger et al., 2017; Scott et al., 2017).

Vanadium forms weak complexes with inorganic components under oxidizing conditions, whereas organic complexes are likely to be reoxidized either in the water column or in sediments under oxic water-column conditions. Consequently, V is not strongly enriched in sediments deposited beneath an oxic water column. By contrast, under anoxic or suboxic conditions, reducing compounds such as H_2S have a high capacity to reduce vanadate to vanadyl and possibly V(III) (Sadiq, 1988), while organic components prone to complexation with reduced V forms are more stable under such conditions. This results in enhanced drawdown efficiency and ultimately V enrichment in sediments deposited under anoxic or suboxic conditions. The sequestration of V(III) can also be enhanced by incorporation into clay minerals at the seafloor or in sediments. In view of this, anoxic and euxinic water column conditions are viewed as favorable environmental conditions for V enrichment during deposition of black shales (Algeo and Maynard, 2008; Bennet and Canfield, 2020; Breit and Wanty, 1991; Huang et al., 2015; Lewan, 1984; Schlesinger et al., 2017; Scott et al., 2017).

In the Francevillian basin, U-ore deposits formed by mixing of U-rich, oxidized fluids (that passed through the FA Formation and probably the underlying Archean basement) and reduced fluids (hydrocarbons migrated from the Francevillian FB Formation black shales) in the FA Formation sandstones (see Section 2 above). Therefore, V enrichment and its association with the Francevillian U-ore deposits could have been caused by either (1)

alteration of V-bearing minerals in the FA Formation sandstones and conglomerates (detrital input) and the Archean basement (e.g., igneous rocks), or (2) migration of V-rich hydrocarbons from the Francevillian FB Formation black shales deposited under reducing conditions.

5.1.1. Detrital and igneous source for V enrichment?

With the exception of U-mineralized structural traps and the contact between the Archean basement and the Francevillian Group, where large volumes of basinal fluids circulated (Mathieu et al., 2000, Ossa Ossa, 2010), V concentrations, in both the FA Formation and the underlying Archean granitoids, are below average upper continental crust value of 97 µg/g (Table 1; Figs. 4, 5). Detrital input during deposition of the FA Formation was the main source for U, REEs (Cuney and Mathieu, 2000; Gauthier-Lafaye and Weber, 1989; Mathieu et al., 2000, 2001; Ossa Ossa, 2010; Ossa Ossa et al., 2014, 2020) and potentially V. It seems plausible that the provenance in different compartments of the basin could have influenced V supply to the Francevillian basin U-ore deposits and thus the occurrence of natural nuclear reactors.

It has previously been shown that weathering of Archean rocks of the North and South Gabon massifs sourced siliciclastic sediments to the Francevillian basin, with Mesoarchean granitoids being the dominant source for U-bearing detrital minerals (Ossa Ossa et al., 2020). Vanadium is enriched in mafic and ultramafic rocks compared to felsic rocks (e.g., Cawthorn et al., 2005; Fischer and Ohl, 1970; Kerr et al., 2013). Therefore, mafic and ultramafic rocks of the Bélinga Group, developed in greenstone belts of the North and South Gabon massifs, could have been potential V sources to the Francevillian basin. This is consistent with higher V enrichments ($V/Al > V/Al_{UCC}$ of ~12) found in these metaigneous rocks compared to other units of the Archean basement, such as granitoids ($V/Al < V/Al_{UCC}$ of ~12; Fig. 5). However,

293 the occurrence of abundant Fe-rich detrital minerals such as titanomagnetite, rutile and
294 chloritized Fe-rich silicate grains in the FA Formation sandstone and conglomerate (Figs. 3A,
295 3B; Bankole et al., 2016; Gauthier-Lafaye and Weber, 1989; Ossa Ossa, 2010; Ossa Ossa et
296 al., 2014), without any clear paleogeographic pattern, suggests that detrital input
297 homogeneously supplied V to the Francevillian basin.

298 Intense alteration processes that affected these V-bearing detrital minerals in the FA
299 Formation (Fig. 3; Ossa Ossa, 2010; Ossa Ossa et al., 2014) suggest that V was mobilized,
300 together with U, by circulating oxidized fluids that led to the formation of the uranium-ore
301 deposits. The western edge of the basin hosts both strongly V-enriched U-ore deposits of
302 Mounana and Boyindzi without natural nuclear reactors, and the less V-enriched, but still above
303 average UCC, U deposits of Oklo-Okelobondo and Bangombé with natural nuclear reactors
304 (Naudet, 1991). However, these two types of U-ore deposits were generated by migration of
305 the same oxidized fluids that had much higher concentrations of U than V. It is thus unlikely
306 that alteration of V-bearing detrital minerals sourced from the Archean Bélinga Group and
307 granitoids, or leaching of the underlying Archean basement by circulating fluids, was
308 responsible for the difference in V enrichment observed between these U deposits.

309

310 *5.1.2. Authigenic V enrichment in the Francevillian basin?*

311 In the Francevillian basin black shales, pronounced V enrichment (V/Al ranges between
312 12 and 77) relative to the average UCC (V/Al_{UCC} = 12) is observed in the FC and FD
313 formations. By contrast, no obvious V enrichment is recorded in the FB Formation (V/Al <
314 V/Al_{UCC}), except for a minor increase corresponding to the Mn-rich Upper FB_1 Member (V/Al
315 ranges between 4 and 18, but with the medium value < V/Al_{UCC}; Fig. 4). Considering that V
316 enrichment in black shales is mainly controlled by the concentration of H_2S, organic

complexation, and incorporation into clay minerals under suboxic to anoxic, and particularly sulfidic, conditions in either seawater or sediment pore-waters (Algeo and Maynard, 2008; Breit and Wanty, 1991; Huang et al., 2015; Lewan, 1984; Schlesinger et al., 2017; Scott et al., 2017), these redox conditions must have developed during deposition of the FC and FD formations and, to some extent, the Upper FB_1 Member.

Deposition of the FB Formation predominantly occurred under oxidized water-column conditions (Canfield et al., 2013; Ossa Ossa et al., 2018). However, a two-step deoxygenation resulted in build-up of dissolved H_2S in the water column during deposition of the Upper FB_1 Member and the FC and FD formations (Ossa Ossa et al., 2018). Specifically, highly negative $\delta^{34}S$ values and lower than 0.22 FeHR/FeT (highly reactive iron / total iron contents) ratios recorded by the FB Formation black shales have been interpreted as representing deposition beneath a well-oxygenated seawater column with a relatively high sulfate concentration (Canfield et al., 2013; Ossa Ossa et al., 2018). The only exception is found in the Upper FB_1 Member, which has positive to near-to-zero $\delta^{34}S$ values, FeHR/FeT ratios fluctuating from below 0.22 to above 0.38, and FePy (pyrite iron)/FeHR ratios both above and below 0.7 (Canfield et al., 2013; Ossa Ossa et al., 2018), indicating episodically euxinic conditions in an otherwise predominantly oxic water column, with a depleted sulfate pool (Figs. 4, 7; Ossa Ossa et al., 2018). Oxic conditions during deposition of the Upper FB_1 Member are also supported by Mn(II) oxidation and precipitation from the water column (Gauthier-Lafaye and Weber, 2003; Ossa Ossa et al., 2018). Highly positive $\delta^{34}S$ values, FeHR/FeT ratios higher than 0.38, FePy/FeHR ratios predominantly above 0.7, and positive $\delta^{98}Mo$ values above 0.8‰ in the FC and FD formation black shales have been linked to the development of widespread euxinic conditions in the Francevillian basin, and potentially the global ocean (Fig. 4; Canfield et al., 2013; Ossa Ossa et al., 2018), with a depleted seawater sulfate reservoir at the end of the Lomagundi carbon isotope excursion (Ossa Ossa et al., 2018).

With vanadate being stable and poorly reactive under oxic conditions (Sadiq, 1988), along with the tendency for organic complexes to be reoxidized in an oxic water column and sediments, the lack of significant V enrichment in the FB Formation black shales might reflect deposition under a well-oxygenated water column. This would explain the low V concentrations with trivial authigenic V enrichments ($V/Al < V/Al_{UCC}$) in the FB Formation black shales (Fig. 4). By contrast, significant V enrichments in the FC and FD formation black shales (V/Al up to 77) are consistent with the buildup of dissolved H_2S in the water column under euxinic conditions. It has been proposed that V concentrations in black shales > 500 ppm reflect V enrichments associated with the development of hyper-euxinic conditions, where dissolved H_2S concentrations approach or exceed ~10 mM (Scott et al., 2017). In modern suboxic and euxinic environments, authigenic V enrichments are as high as 300 ppm (Brumsack, 2006; Piper and Dean, 2002), reflecting removal of dissolved V from seawater as vanadyl (Breit and Wanty, 1991). However, H_2S concentrations as high as 8 mM in the modern marine Framvaren Fjord environments are not accompanied by high V enrichments in sediments, with V concentrations at ~41 ppm (Skei et al., 1988). This suggests that H_2S concentrations likely commonly have to be at least >8 mM in order to produce significant V enrichments (Scott et al., 2017). Furthermore, thermodynamic calculations predict that vanadate reduction to V(III) should bypass vanadyl formation if H_2S concentrations exceed 0.029 mM (Wanty and Goldhaber, 1992). V concentrations in some of the FC and FD formation black shales exceed 500 ppm and, similar to other trace metals (e.g., Mo, U, Cr), are much higher than in the FB Formation black shales and average upper continental crust (see Fig. 4 and Canfield et al., 2013). This suggests that dissolved seawater H_2S concentrations during deposition of the FC and FD Formation black shales likely exceeded 8 mM, and in most cases dissolved V was reduced to V(III).

Seawater redox conditions at the end of the Lomagundi carbon isotope excursion in the Francevillian Basin (i.e., anoxic and hyper-euxinic), enhanced the drawdown efficiency of V resulting in significant enrichments in the FC and FD formation black shales. Importantly, a two-step deoxygenation has previously been proposed, with a decreased seawater sulfate reservoir during deposition of the Upper FB_{1c} Unit. Even lower seawater sulfate concentrations then occurred during deposition of the FC and FD formations in the aftermath of the Lomagundi carbon isotope excursion (Ossa Ossa et al., 2018). Here, minor V enrichment in the Upper FB_{1c} Unit and significant V enrichment in the FC and FD formations further support more pronounced reducing conditions and higher dissolved seawater H_2S concentrations during deposition of the Upper Francevillian Group (straddling the end and aftermath of the Lomagundi carbon isotope excursion), compared with the major event of Mn precipitation in the Upper FB_{1c} Unit (during the Lomagundi carbon isotope excursion). However, the record of the Lomagundi carbon isotope excursion and its end in the Francevillian Group was challenged in a recent study (Bakakas-Mayika et al., 2020). This work used sedimentological observations for the LST12 drill core (see Fig. 1) to argue that the Upper FC_1 Member inferred to record the end of the Lomagundi carbon isotope excursion (see Fig. 2 in Ossa Ossa et al., 2018) corresponds to deep-water carbonate deposits (Unit V in Fig. 2 of Bakakas-Mayika et al., 2020). Based on their reinterpretation of sedimentary structures, Bakakas-Mayika et al. (2020) concluded that the highly positive carbon isotope values recording in this drill core reflect a local signal of a shallow-marine evaporite environment, whereas contemporaneous, open-marine deep-waters do not carry this signal. However, crinkly laminated dolostones with well-preserved microbial mat structures in the Upper FC_1 Member indicate deposition in a shallow-marine environment (see Fig. 2 in Ossa Ossa et al., 2018). Furthermore, thin carbonate beds in deep-water black shales of the FB Formation also record positive $\delta^{13}C_{carb}$ values (El Albani et al., 2010; Ossa Ossa et al., 2013, 2018). These data demonstrate that deep-water settings in the

391 Francevillian Basin record the Lomagundi carbon isotope excursion (El Albani et al., 2010;
392 Ossa Ossa et al., 2013, 2018), whereas unit V reflects its end, with associated deoxygenation
393 of Paleoproterozoic oceans. The V-enrichment in the FC and FD formation black shales thus
394 reflects deoxygenation of the Paleoproterozoic oceans at the end of the Lomagundi carbon
395 isotope excursion, and this was a source of V for the Francevillian Basin U-ore deposits. By
396 contrast, the V-poor FB Formation black shales, deposited under oxygenated marine conditions
397 during the Lomagundi carbon isotope excursion, would not have provided V to these U-ore
398 deposits.

399

400 *5.2. Hydrocarbon migration pathways and V redistribution in the FA Formation U-ore*
401 *deposits*

402 Vanadium is a common component of hydrocarbon fluids, especially asphaltic oils
403 (e.g., Fischer and Ohl, 1970). Hydrocarbon fluids were previously described to have migrated
404 from the organic-rich FB Formation petroleum source rocks to the FA Formation sandstone
405 reservoirs along faults (Fig. 2; Gauthier-Lafaye, 1986; Gauthier-Lafaye and Weber, 1989,
406 2003; Mathieu et al., 2000; Ossa Ossa, 2010; Ossa Ossa et al., 2014; Weber et al., 2016).
407 However, hydrocarbon generated from the V-poor FB Formation black shales cannot account
408 for the high V enrichments recorded by the FA Formation U-ore deposits. More recently, it has
409 been shown that the FC and FD Formation black shales also generated significant quantities of
410 hydrocarbons in the Francevillian Basin (Ossa Ossa et al., 2018). Although rock-eval pyrolysis
411 data for the Francevillian Group black shales indicate advanced post-depositional
412 transformation and over-maturation of the organic matter (Fig. 6A), concentrations of V, Ni
413 and S suggest that these petroleum source rocks are mainly characterized by type II oil-prone
414 kerogen with a minor contribution from type III gas-prone kerogen (Fig. 6B). This is consistent

415 with the proposed scenario of oil generation from the Francevillian Group black shales and its
416 migration to the FA Formation sandstone reservoirs at ca. 2.05 Ga during the ca. 2.2-2.0 Ga
417 Eburnian Orogeny (e.g., Gauthier-Lafaye, 1989; Gauthier-Lafaye and Weber, 1989; Gauthier-
418 Lafaye et al., 1996; Weber et al., 2016).

419 Mobilization and accumulation of hydrocarbons in the Franceville sub-basin was
420 controlled by faults and associated structural traps (Fig. 8). Uranium-ore deposits of Oklo-
421 Okelobondo and Bangombé are surrounded by the FB Formation mudstones, which served as
422 a seal, and NW-SE and N-S trending faults related to the structural trap formation (Gauthier-
423 Lafaye and Weber, 1989) allowed hydrocarbon migration only from the FB Formation black
424 shales (Fig. 8B). By contrast, the same NW-SE and N-S trending faults connected U deposits
425 of Boyindzi, Mounana and Mikouloungou with both the FB Formation and the FC and FD
426 formations, allowing hydrocarbon migration (Fig. 8B). This indicates that U-ore deposits
427 lacking natural nuclear reactors in the Francevillian basin could have been directly or indirectly
428 connected to an external source of V, represented by the FC and FD formation black shales
429 through the regional fault system (Fig. 8A). High V concentrations in these U-ore deposits (up
430 to 1.5 wt.%) likely correspond to authigenic V enrichment in the source rocks from which
431 hydrocarbons migrated. Migration of V-rich hydrocarbons from the FC and FD formation black
432 shales could have helped to prevent natural fission reactions in some of the Francevillian basin
433 U-ore deposits, thus limiting the regional impact of the Oklo natural nuclear reactors.

434

435 *5.3. Implications for the extent of development of natural nuclear fission reactors*

436 Broadly coeval polymetallic V-rich sedimentary U-ore deposits, which formed in a
437 similar geological setting to those of the Francevillian basin (e.g., Mounana, Boyindzi,
438 Mikouloungou), are found in the Karelia Craton of the Fennoscandian Shield (Boitsov, 1995;

439 Boitsov and Nikolsky, 1997; Cuney, 2010; Molnár et al., 2017). For example, in the Onega
440 basin, several high-grade U-ore deposits (UO_2 up to 0.13 wt.%) with associated high V
441 concentrations up to 4.22 wt.% (i.e., Srednyaya Padma, Verkhnyaya Padma, Tsarevskoe,
442 Vesennee, Kosmozerskoe and Shul'ginovskoe), are also linked to the solidified petroleum
443 (shungite) hosted in structural traps (Boitsov, 1995; Negrutsa and Polekhovsky, 1995).
444 Importantly, all of these deposits are stratigraphically restricted to the contact of the Zaonega
445 Formation reduced, organic matter-rich sediments with oxidized carbonates and red beds of the
446 Tulomozero Formation (Golubev and Novikov, 2005). In the Onega basin, mineralizing
447 metasomatic events have been dated at ~1770, 1740 and 1640 Ma (Borozdin et al., 2014 and
448 references therein), by which time the $^{235}U/^{238}U$ ratio was no longer high enough to allow
449 natural fission reactions (e.g., Gauthier-Lafaye and Weber, 1989, 2003).

450 However, similar to the Francevillian U-ore deposits, mineralization in the Onega basin
451 is likely the consequence of multiple metasomatic events, and the age record of the oldest
452 mineralization event might have been overprinted by younger fluid circulation. Borozdin et al.
453 (2014) dated mineralizing metasomatic events between 1740 and 1640 Ma using the Rb-Sr
454 isochron method on whole-rock samples and gangue mineral separates. Accurate determination
455 of the mineralization age of U deposits generally requires the use of modern high-resolution *in*
456 *situ* isotopic dating techniques, such as U-Pb SIMS or LA-ICP-MS on uraninite, that date
457 micrometre-scale ore mineral zones unaffected by later metasomatic events (cf. Cuney and
458 Kyser, 2008). The Rb-Sr isotope system used by Borozdin et al. (2014) is highly sensitive to
459 re-equilibration with late metasomatic fluids. Moreover, such a method only dates the
460 associated metasomatic minerals, and not the U mineralization itself. Hydrocarbon-bearing
461 polymetallic U-ore deposits in the Peräpohja Belt of the Karelia Craton, Finland (Molnár et al.,
462 2017) formed at ca. 2.03-2.01 and 1.95-1.94 Ga, whereas later, metasomatic U-mineralizing
463 events related to the Svecofennian Orogeny reset the U-Pb system at ca. 1.91-185, 1.85 and

1.80 Ga (Molnár et al., 2017). Although the latter case shows that the Karelian U-ore deposits formed as early as ca. 2.03-2.01 Ga, when $^{235}U/^{238}U$ ratios were high enough for natural fission reactions to occur (cf. Gauthier-Lafaye and Weber, 1989, 2003), a detailed and high-resolution geochronological study of U deposits from the Onega basin is needed to determine the exact age of the oldest U mineralization event.

High V concentrations (up to 957 ppm), along with U and Mo concentrations up to 36 and 180 ppm, respectively, occur in black shales of the Upper Zaonega Formation (Asael et al., 2018). These concentrations indicate significant V enrichment, which is achievable only under hyper-euxinic conditions with dissolved seawater H_2S level likely exceeding ~8 mM (cf. Scott et al., 2017). Deposition of these black shales is also inferred to have occurred under deoxygenated seawater conditions at the end of the Lomagundi carbon isotope excursion (e.g., Canfield et al., 2013; Kump et al., 2011; Melezik et al., 2007; Scott et al., 2014). These marine redox conditions are further supported by Mo isotope data from these black shales, suggesting extensive development of strongly euxinic conditions in the mid-Paleoproterozoic ocean at the end of the Lomagundi carbon isotope excursion (Asael et al., 2018).

However, an alternative view proposed that redox processes in the Francevillian and Onega basins reflect local rather than global processes in the mid-Paleoproterozoic oceans (e.g., Paiste et al., 2020a, 2020b; Melezhik et al., 1999). Based on trace metal enrichments (U, Mo, Re) and large U isotope fractionations found in black shales of the Zaonega Formation, a recent study proposed that the Paleoproterozoic ocean remained well-oxygenated after the end of the Lomagundi carbon isotope excursion (Mänd et al., 2020). Mänd et al. (2020) further argued that Mo isotope signature of the Zaonega Formation, previously interpreted to reflect widespread anoxic conditions in the Paleoproterozoic oceans in the aftermath of the GOE (Asael et al., 2018), can also be reconciled with well-oxygenated seawater conditions. These views are clearly inconsistent with the widespread aspect of V hyper-enrichment in the

Paleoproterozoic sediments in the aftermath of the Lomagundi carbon isotope excursion. We thus provide a different perspective below on: 1) the age of the Onega basin succession, specifically the Tulomozero and Zaonega formations; 2) the age of the sills within the Zaonega Formation and whether water-column methane was thermochemically released from organic-rich shales or biologically produced in the basin; 3) redox structure within the basin during deposition of the Zaonega Formation; 4) tectonic setting of the basin and its isolation from the ocean; and 5) whether this basin records global or local geochemical signals.

The extensively cited date of 1975.3 ± 2.8 Ma (U–Pb ID-TIMS analysis of single zircon grains), previously interpreted to correspond to syn-sedimentary volcanic eruption at the base of the Jatulian Group in the Onega basin (which records the Lomagundi carbon isotope excursion; Martin et al., 2015), has recently been linked to sill emplacement and is thus younger than the depositional age of the Tulomozero Formation (cf. Paiste et al., 2020b). All other ages compiled in Martin et al. (2015) are for sills and dykes in the Zaonega Formation, and thus only provide a minimum age for this unit. The only exception is the 1982 ± 4.5 Ma date for a tuff in the basal part of the Zaonega Formation (Martin et al., 2015). However, this date is based on only one zircon grain ID-TIMS U-Pb analysis, with all other (~30) grains being either discordant or Archean in age. On the another hand, ca. 2.05 Ga Re-Os dates were independently reported for the middle part of the Zaonega Formation by Hannah et al. (2008) and Bauer et al. (2020); these dates have not yet been presented in peer-review literature and should be used with caution. The same applies to U-Pb dating of zircon from volcanic tuffs of the Upper Francevillian Group that yielded dates of 2083 ± 6 Ma (SHRIMP; Horie et al., 2005) and 2072 ± 29 Ma (LA-ICP-MS; Bouton et al., 2009). It is thus clear that robust depositional age constraints are currently unavailable for the Francevillian and Onega basins. Considering uncertainty in depositional ages of the Zaonega Formation and the Francevillian Group, it seems premature to argue based solely on available geochronologic constraints whether these

514 successions are correlative or not. Nevertheless, both successions record the end of the carbon
515 isotope excursion before ca. 2.05 Ga and, considering that presently available
516 chemostratigraphic and geochronologic data indicate the end of a single, long-lasted C isotope
517 excursion at this time interval, it is most parsimonious to infer that both the Upper Francevillian
518 Group and the Zaonega Formation reflect the end of the Lomagundi carbon isotope excursion
519 between ca. 2.11 and 2.06 Ga (cf. Karhu and Holland, 1996; Melezhik et al., 2015; Ossa Ossa
520 et al., 2018).

521 Syn-depositional emplacement of sills and dykes into unlithified sediments of the
522 Zaonega Formation have been used as an argument for thermochemical methane generation in
523 the Onega basin during deposition of the Zaonega Formation (e.g., Qu et al., 2012, 2018). The
524 peperites on contacts of intrusions and sediments have not been fully documented in published
525 literature (tar balls are not reported from the Zaonega Formation and yet are ubiquitous in the
526 unconformably overlying Kondopoga Formation; e.g., Melezhik et al., 1999), and in any case,
527 shallowly buried sediments can remian unlithified for millions of years until affected by
528 regional metamorphism. More relevant, despite extensive dating of dykes and sills in the
529 Zaonega Formation (e.g., Martin et al., 2015), no 2.1-2.0 Ga dates, corresponding to the
530 inferred age of the Zaonega Formation (see above), have thus far been reported. We thus infer
531 that robust evidence for thermochemical methane generation in the Onega basin during
532 deposition of the Zaonega Formation is lacking. Instead, organic-rich facies of the Zaonega
533 Formation and their highly negative $\delta^{13}C_{org}$ values indicate biological methane production and
534 recycling (methanogenesis and methanotrophy) in the Onega basin. Combined biological
535 methane cycling in the Onega basin, high rates of organic carbon loading, enrichment in redox-
536 sensitive elements, and Fe and Mo isotope values indicate deposition of the Zaonega Formation
537 in a redox-stratified basin (cf. Asael et al., 2018; Mänd et al., 2021).

538 The tectonic setting of the Onega basin and its connection to the global ocean,
539 especially during deposition of the Zaonega Formation, is poorly constrained and widely
540 debated (e.g., Melezhik et al., 1999, 2015; Melezhik and Hanski, 2012; Negrutsa, 1984;
541 Ojakangas et al., 2001). However, regional lithostratigraphic correlations among presently
542 structurally confined basins suggest that a passive continental margin with shallow-marine
543 carbonate-evaporite-red bed deposits established over the Karelia Craton in the Upper Jatulian,
544 with paleocurrents predominantly north-to-west pointing towards deep-water, open-marine
545 settings (Ojakangas et al., 2001). These passive-margin, shallow-marine successions, recording
546 the Lomagundi carbon isotope excursion (e.g., Karhu, 1993), are sharply overlain, with an
547 erosional surface overlain by organic-rich dolostones, marls and shales (Galdobina, 1987)
548 indicating craton-wide drawning of carbonate platform, likely in response to tectonic
549 reorganization. The thickness of black shales decreases to the north-northwest, consistent with
550 the sediment provenance to the south (cf. Melezhik et al., 2015). In contrast to the widely used
551 model of 'rift-bound lagoon' in the regional literature for the Onega basin during deposition of
552 the Zaonega Formation (Melezhik et al., 1999. 2015), we favor a deeper-water, marine setting
553 during deposition of the Zaonega Formation (cf. Negrutsa, 1984; Ojakangas et al., 2001), with
554 largely unrestricted exchange with the global ocean.

555 Geochemical models for the Zaonega Formation, based largely on trace metal
556 enrichments in the black shales (e.g., Mänd et al., 2020, 2021; Paiste et al., 2020a, 2020b), also
557 converge on the view that the Onega basin was likely well-connected to the Paleoproterozoic
558 ocean. In order to provide new insight into whether biogeochemical processes in the Onega
559 and Francevillian basins reflect local processes in restricted marine settings or deposition in
560 marine basins well-connected to the Paleoproterozoic ocean, V/Al vs. Mo/Al and V/Al vs. U/Al
561 cross-plots (Fig. 9), based on variations observed in modern environments, may be used
562 (Bennet and Canfield, 2020). An extensive study of open-marine and restricted modern

563 environments, with various redox conditions, has demonstrated that V/Al > 46 µmole/mole can
564 only be reached in an open-marine setting with perennial anoxia (Bennet and Canfield, 2020).
565 Data for the Upper Zaonega Formation and Upper Francevillian Group are dominated by V/Al
566 > 46 µmole/mole (Fig. 9). Furthermore, the cross-plots show positive correlations between
567 V/Al and Mo/Al, and between V/Al and U/Al (Fig. 9). The positive correlations also highlight
568 a stratigraphic trend from oxic-to-suboxic, to ferruginous-to-euxinic water-column conditions
569 from the FC to FD Formation in the Francevillian basin, and from the lower to upper part of
570 the Upper Zaonega Formation in the Onega basin (Fig. 9). These trends indicate that V hyper-
571 enrichment developed gradually as a result of progressive deoxygenation during deposition of
572 these two sedimentary successions, as previously proposed (Asael et al., 2018; Canfield et al.,
573 2013; Kump et al., 2011; Scott et al., 2014; Ossa Ossa et al., 2018) for marine basins well-
574 connected to the Paleoproterozoic oceans (cf., Algeo and Lyons, 2006; Bennet and Canfield,
575 2020; Scott et al., 2017).

576 In contrast to the recent suggestion (e.g., Mänd et al., 2020), largely based on extreme
577 enrichments in redox-sensitive elements (Mo, U, Re) and U isotope fractionations, we infer
578 that these stratigraphic trends reflect ocean deoxygenation in the aftermath of the Lomagundi
579 carbon isotope excursion, rather than continuation of the oxygen overshoot. Importantly, the
580 occurrence of at least six major U-V polymetallic deposits and multiple showings hosted in the
581 basal Zaonega Formation of the eastern part of the Onega basin, which was previously studied
582 to infer marine redox conditions, suggest that caution should be exercised in interpreting these
583 data, since redox-front deposits are known to develop extreme degrees of enrichment in redox-
584 sensitive elements via multi-stage reduction-oxidation cycles, and extreme isotopic
585 fractionation of redox-sensitive elements (e.g., U, Mo, Fe) could be generated under these
586 conditions. The point is that although the stratigraphical level with extreme enrichments in
587 redox-sensitive elements and U isotope fractionation is in the upper part of the Zaonega

588 Formation and stratigraphically far from U-V polymetallic deposits hosted at the base of the
589 unit, tectonic and magmatic drivers for fluid circulation and hydrocarbon generation, as well
590 as redox gradients between organic-rich and highly oxidized sediments, were in place to induce
591 enrichments and isotopic fractionation in redox-sensitive elements and to trap metal-rich
592 hydrocarbon-bearing fluids at the contact of lithologies with different porosity and
593 permeability.

594 Efficient V removal from seawater to sediments during expanded anoxia and euxinia
595 in the mid-Paleoproterozoic ocean at the end, and in the aftermath, of the Lomagundi carbon
596 isotope excursion, appears to have contributed to the formation of V-rich black shales, an
597 important source for hydrocarbon generation in the Francevillian and Onega basins, and
598 probably in other localities across the globe. Hydrocarbons generated from these V-rich black
599 shales played a key role in preventing natural fission reactors from broader expression in ca.
600 2.06-1.9 Ga high-grade U-ore deposits at a time when natural $^{235}U/^{238}U$ ratios were still above
601 the critical threshold of 0.03, which is required for natural fission reactions. Because the
602 Francevillian and Onega basins both record petroleum migration to structural and stratigraphic
603 traps and high-grade U-ore mineralization, V enrichment in the petroleum-source rocks (black
604 shales deposited during the mid-Paleoproterozoic ocean deoxygenation) and hydrocarbons
605 derived from them helped prevent wider expression of natural nuclear reactors, at least on the
606 scale of the Francevillian basin.

607

608 **6. Conclusions**

609 Vanadium enrichment in Francevillian U-ore deposits was derived from (1) altered V-
610 bearing minerals of the detrital fraction in the FA Formation sandstones and conglomerates
611 and/or Archean mafic and ultramafic igneous rocks of the Archean basement underneath the

mid-Paleoproterozoic Francevillian basin, and (2) authigenic enrichment in the FC and FD formation black shales deposited under expanded euxinic conditions. Hydrocarbons migrated from these V-rich black shales into structural traps and established a redox front that maintained U precipitation in the upper part of the FA Formation, also providing an additional source of V to some of the Francevillian Group U-ore deposits. Hydrocarbon migration pathways along major faults suggest that U-ore deposits hosting natural nuclear reactors (Oklo-Okelobondo and Bagombé) were formed at a redox front maintained by hydrocarbons generated from the FB Formation V-poor black shales. By contrast, those without natural nuclear reactors were controlled by hydrocarbons derived from both the FB V-poor black shales and the FC and FD formation V-rich black shales.

The FB Formation petroleum-source rocks are V-poor since they were deposited in a well-oxygenated mid-Paleoproterozoic shallow-marine setting during the Lomagundi carbon isotope excursion. Enrichment in V in the FC and FD formation black shales reflects deposition in anoxic and hyper-euxinic marine environments during, and in the aftermath, of ocean deoxygenation at the end of the mid-Paleoproterozoic Lomagundi carbon isotope excursion. Hydrocarbon migration from the V-rich petroleum-source rocks along regional fault system led to high V concentrations in some U-ore deposits, preventing development of natural nuclear reactors. Potentially coeval, high-grade, U-V polymetallic mineralization hosted in the Onega basin in Karelia, Russia in association with black shales deposited at the end, and in the aftermath, of the Lomagundi carbon isotope excursion, further suggest that mid-Paleoproterozoic ocean deoxygenation helped prevent natural nuclear reactors from reaching a wider expression.

Acknowledgments:

FOO and RS acknowledge financial support from the University of Tuebingen and the German Research Foundation DFG (Grant SCHO1071/11-1). The National Research Foundation of South Africa is thanked by AH (Grant 75892). Participation by AB was supported by Discovery and Accelerator Grants from the Natural Sciences and Engineering Research Council of Canada (NSERC). SWP acknowledges support from a Royal Society Wolfson Research Merit Award.

References

Albut, G., Babechuk, M. G., Kleinhanns, I. C., Benger, M., Beukes, N. J., Steinhilber, B., Smith, A. J. B., Kruger, S. J., Schoenberg, R., 2018. Modern rather than Mesoarchaean oxidative weathering responsible for the heavy stable Cr isotopic signatures of the 2.95 Ga old Ijzermijn iron formation (South Africa). *Geochimica Cosmochimica Acta* **228**, 157–189.

Algeo, T.J., Maynard, J.B., 2008. Trace-metal covariation as a guide to water-mass conditions in ancient anoxic marine environments. *Geosphere* **4**, 872–887.

Algeo, T.J., Lyons, T.W., 2006. Mo-total organic carbon covariation in modern anoxic marine environments: implications for analysis of paleoredox and paleohydrographic conditions. *Paleoceanography and Paleoclimatology* **21**, DOI: 10.1029/2004PA001112.

Asael, D., Rouxel, O., Poulton, S. W., Lyons, T. W., Bekker, A., 2018. Molybdenum record from black shales indicates oscillating atmospheric oxygen levels in the early Paleoproterozoic. *American Journal of Science* **318**, 275–299.

Babechuk, M.G., Kamber, B.S., Greig, A., Canil, D., Kodolanyi, J., 2010. The behaviour of tungsten during mantle melting revisited with implications for planetary differentiation time scales. *Geochimica Cosmochimica Acta* **74**, 1448–1470.

Babechuk, M. G., Widdowson, M., Murphy, M., Kamber, B. S., 2015. A combined Y/Ho, high field strength element (HFSE) and Nd isotope perspective on basalt weathering, Deccan Traps, India. *Chemical Geology* **396**, 25–41.

Bakakas-Mayika, K., Moussavou, M., Prave, A. R., Lepland, A., Mbina, M., Kirsimäe, K., 2020. The Paleoproterozoic Francevillian succession of Gabon and the Lomagundi-Jatuli event. Geology 48, https://doi.org/10.1130/G47651.1.

Bankole, O.M., El Albani, A., Meunier, A., Rouxel, O.J., Gauthier-Lafaye, F., Bekker, A., 2016. Origin of red beds in the Paleoproterozoic Franceville basin, Gabon, and implication for sandstone-hosted uranium mineralization. *American Journal of Science* **316**, 839–872.

Bankole, O. M., El Albani, A., Meunier, A., Gauthier-Lafaye, F., 2015. Textural and paleo-fluid flow control on diagenesis in the Paleoproterozoic Franceville basin, South Eastern, Gabon. *Precambrian Research* **268**, 115–134.

Bankole, O. M., El Albani, A., Meunier, A., Poujol, M., Bekker, A., 2020. Elemental geochemistry and Nd isotope constraints on the provenance of the basal siliciclastic succession of the middle Paleoproterozoic Francevillian Group, Gabon. *Precambrian Research* **348**, 105874.

Bauer, A. M., Rooney, A. D., Lepland, A., 2020. Os and Nd isotope constraints on Paleoproterozoic global events as recorded in sediments from Russian Fennoscandia. *AGU Fall Meeting*, December 2020.

Bekker, A., 2014. Lomagundi Carbon Isotope Excursion. In: *Encyclopedia of Astrobiology, Springer-Verlag*, 1–6.

Bennet, W. W., Canfield, D. E., 2020. Redox-sensitive trace metals as paleoredox proxies: A review and analysis of data from modern sediments. *Earth-Science Reviews* **204**, 103175.

Bentridi, S-E., Gall, B., Gauthier-Lafaye, F., Seghour, A., Medjadi, D-E., 2011. Génèse et évolution des réacteurs nucléaires fossiles d'Oklo. *Comptes Rendus Géoscience* **343**, 738–748.

Boitsov, A.V., 1995. The Mineral composition and the ore types of uranium-vanadium deposit Srednaya Padma (Onega region, Russia Federation). In: Changes and events in uranium deposit development, exploration, resources, production and the world supply-demand relationship. *Proceedings of a Technical Committee meeting jointly organized by the International Atomic Energy Agency and the OECD Nuclear Energy Agency*, Kiev. **IAEA-TECDOC-961**, 259–269.

Boitsov, A.V., Nikolsky, A.L., 1997. Characteristics of uranium districts of the Russian Federation. In: Assessment of uranium deposit types and resources —a worldwide perspective. *Proceedings of a Technical Committee meeting jointly organized by the International Atomic Energy Agency and the OECD Nuclear Energy Agency*, Vienna. **IAEA-TECDOC-1258**, 61–75.

Bonhomme, M.G., Gauthier-Lafaye, F. & Weber, F., 1982. An example of lower Protero-zoic sediments – the Francevillian in Gabon. *Precambrian Research* **18**, 87–102.

Bouton, P., Thiéblemont, D., Gouin, J., Cocherie, A., Guerrot, C., Tegyey, M., Préat, A., Simo Ndounze, S., Moussavou, M., 2009. Notice explicative de la Carte géologique de la République du Gabon à 1/200 000, feuille Franceville-Boumango. *Eds DGMC – Ministère des Mines, du Pétrole, des Hydrocarbures*, Libreville, pp. 79.

Borozdin, A. P., Polekhovskii, Y. S., Bushmin, S. A., Glebovitskii, V. A., Belyatskii, B. V., Savva, E. V., 2014. Age of Metasomatism and Ore Formation in the Srednyaya Padma Vanadium–Precious Metals–Uranium Deposit (Karelia, Baltic Shield). *Doklady Akademii Nauk* **454**, 310–314. DOI: 10.1134/S1028334X14010176.

Breit, G.N., Wanty, R.B., 1991. Vanadium accumulation in carbonaceous rocks: a review of geochemical controls during deposition and diagenesis. Chemical Geology **91**, 83–97.

Bros, R., Stille, P., Gauthier-Lafaye, F., Weber, F., Clauer, N., 1992. Sm-Nd isotopic dat-ing of Proterozoic clay material: an example from the Francevillian sedimentary series, Gabon. *Earth and Planetary Science Letters* **113**, 207–218.

Brumsack, H.-J., 2006. The trace metal content of recent organic carbon-rich sediments: implications for Cretaceous black shale formation. *Palaeogeography, Palaeoclimatology, Palaeoecology* **232**, 344–361.

Canfield, D. E., Ngombi-Pemba, L., Hammarlund, E., Bengtson, S., Chaussidon, M., Gauthier-Lafaye, F., Meunier, A., Riboulleau, A., Rollion-Bard, C., Rouxel, O., Asael, D., Pierson-Wickmann, A-C., El Albani, A, 2013. Oxygen dynamics in the aftermath of the Great Oxidation of Earth's atmosphere. *Proceedings of the National Academy of Sciences USA* **110**, 16736–16741.

Cawthorn, R.G., Barnes, S.J., Ballhaus, C., Malitch, K.N., 2005. Platinum Group Element, Chromium, and Vanadium Deposits in Mafic and Ultramafic Rocks. *Economic Geology* **100th Anniversary Volume**, 215–249.

Cuney, M., 2010. Evolution of Uranium Fractionation Processes through Time: Driving the Secular Variation of Uranium Deposit Types. *Economic Geology* **105**, 553–569.

Cuney, M., Kyser K., 2008. Recent and not-so-recent developments in uranium deposits and implications for exploration. *Mineralogical Association of Canada Short Course Series* **39**, p.258.

Cuney, M., Mathieu, R., 2000. Extreme light rare earth element mobilization by diagenetic fluids in the geological environment of the Oklo natural reactor zones, Franceville basin, Gabon. *Geology* **28**, 743–746.

Dembicki, H. J., 2009. Three common source rock evaluation errors made by geologists during prospect or play appraisals. *American Association of Petroleum Geologists Bulletin* **93**, 341– 356.

El Albani, A. *et al*., 2010. Large colonial organisms with coordinated growth in oxygenated environments 2.1 Gyr ago. *Nature* **466**, 100–104.

Fischer, R.P., Ohl, J.P., 1970. Bibliography on the geology and resource of vanadium to 1968. *Geological Survey Bulletin 1316*, United States Government Printing Office, Washington, pp. I–XXXII.

Galdobina, L. P., 1987. The ludicovian super-horizon. In: Sokolov, V.A. (Ed.), Geology of Karelia. Nauka (Science), Leningrad, pp. 59–67 (in Russian).

Gauthier-Lafaye, F., 1986. Les gisements d'uranium du Gabon et les réacteurs d'Oklo. Modèle métallogénique de gîtes à fortes teneurs du Protérozoique inférieur. *Strasbourg, France, Université Louis Pasteur, Ph. D. thesis*, 206 p.

Gauthier-Lafaye, F., 2002. Des analogues naturels de sites de stockage de déchets nucléaires vieux de 2 milliards d'années : les réacteurs de fission nucléaire naturels du Gabon (Afrique). *Comptes Rendus Physique* **3**, 839–849.

Gauthier-Lafaye, F., 2006, Time constraint for the occurrence of uranium deposits and natural nuclear fission reactors in the Paleoproterozoic Franceville Basin (Gabon). *Geological Society of America Memoirs* **198**, 157–167.

Gauthier-Lafaye, F., Holliger, P., Blanc, P. L., 1996. Natural fission reactors in the Franceville basin, Gabon: A review of the conditions and results of a "critical event" in a geologic system. *Geochimica et Cosmochimica Acta* **60**, 4831–4852.

Gauthier-Lafaye, F., Weber, F., 1989. The Francevillian (Lower Proterozoic) uranium ore deposits of Gabon. *Economic Geology* **84**, 2267–2285.

Gauthier-Lafaye, F., Weber, F., 2003. Natural nuclear fission reactors: time constraints for occurrence, and their relation to uranium and manganese deposits and to the evolution of the atmosphere. *Precambrian Res.* **120**, 81–100.

Golubev, A. I., Novikov, Y. N., 2005. Geology of uranium-vanadium deposits of the Transonega region. In: Ieshko, E.P. (Ed.), Environmental problems associated with exploitation of the Srednaja Padma deposit. Karelian Research Centre, Petrozavodsk, pp. 4–13 (in Russian).

Hannah, J.L., Stein, H., Yang, G., Zimmerman, A., Melezhik, V.A., Filippov, M., Turgeon, S.C., Creaser, R., 2008. Re–Os geochronology of a 2.05 Ga fossil oil field near Shunga, Karelia, NW Russia. In: *33rd International Geological Congress*, Oslo, 2008.

Hatch, J. R., Leventhal, J. S., 1992. Relationship between inferred redox potential of the depositional environment and geochemistry of the Upper Pennsylvanian (Missourian) Stark Shale Member of the Dennis Limestone, Wabaunsee County, Kansas, USA. *Chemical Geology* **99**, 65–82.

Horie, K., Hidaka, H., Gauthier-Lafaye, F., 2005. U-Pb geochronology and geochemistry of zircon from the Franceville series at Bidoudouma, Gabon. *Geochimica et Cosmochimica Acta* **69**, A11.

Huang, J-H., Huang, F., Evans, L., Glasauer, S., 2015. Vanadium: Global (bio)geochemistry. *Chemical Geology* **417**, 68–89.

Jensen, K.A., Ewing, R. C., 2001. The Okélobondo natural fission reactor, southeast Gabon: Geology, mineralogy, and retardation of nuclear-reaction products. *Geological Society of America Bulletin* **113**, 32–62.

781 Karhu, J. A., 1993. Palaeoproterozoic evolution of the carbon isotope ratios of sedimentary
782 carbonates in the Fennoscandian Shield. *Geological Survey of Finland Bulletin* **371**,
783 1–87.
784 Karhu, J. A., Holland, H. D., 1996. Carbon isotopes and the rise of atmospheric oxygen.
785 *Geology* **24**, 867–870.
786 Kerr, A., Walsh, J.A., Sparkes, G.W., Hinchey, J.G., 2013. Vanadium potential in
787 Newfoundland and Labrador: A review and assessment. *Newfoundland and Labrador*
788 *Department of Natural Resources Geological Survey,* **Report 13–1**, 137–165.
789 Kump, L. R., Junium, C., Arthur, M. A., Brasier, A., Fallick, A., Melezhik, V., Lepland, A.,
790 Črne, A. E., Luo, G., 2011. Isotopic Evidence for Massive Oxidation of Organic
791 Matter Following the Great Oxidation Event. *Science* **334**, 1694–1696.
792 Lecomte, A., Michels, R., Cathelineau, M., Morlot, C., Brouand, M., Flotté, N., 2020.
793 Uranium deposits of Franceville basin (Gabon): Role of organic matter and oil
794 cracking on uranium mineralization. *Ore Geology Reviews* **123**, 103579. DOI:
795 10.1016/j.oregeorev.2020.103579.
796 Lewan, M. D., 1984. Factors controlling the proportionality of vanadium and nickel in crude
797 oils. *Geochimica et Cosmochimica Acta* **48**, 2231–2238.
798 Mänd, K. *et al*., 2020. Palaeoproterozoic oxygenated oceans following the Lomagundi–Jatuli
799 Event. *Nature Geoscience* **13**, 302–306.
800 Mänd, K., Lalonde, S.V., Paiste, K., Thoby, M., Lumiste, K., Robbins, L. J., Kreitsmann, T.,
801 Romashkin, A. E., Kirsimäe, K., Lepland, A., Konhauser, K. O., 2021. Iron Isotopes
802 Reveal a Benthic Iron Shuttle in the Palaeoproterozoic Zaonega Formation: Basinal
803 Restriction, Euxinia, and the Effect on Global Palaeoredox Proxies. *Minerals* **11**, 368.
804 DOI: 10.3390/min11040368.
805 Martin, A. P., Prave, A. R., Condon, D. J., Lepland, A., Fallick, A. E., Romashkin, A. E.,
806 Medvedev, P. V., Rychanchik, D. V., 2015. Multiple Palaeoproterozoic Carbon Burial
807 Episodes and Excursions. *Earth and Planetary Science Letters* **424**, 226–236.
808 Mathieu, R., Cuney, M., Cathelineau, M., 2000. Geochemistry of palaeofluids circulation in
809 the Franceville basin and around Oklo natural nuclear reaction zones (Gabon).
810 *Journal of Geochemical Exploration* **69**, 245–249.
811 Mathieu, R., Zetterstrom, L., Cuney, M., Gauthier-Lafaye, F., Hidaka, H., 2001. Alteration of
812 monazite and zircon and lead migration as geochemical tracers of fluid
813 paleocirculations around the Oklo-Okelobondo and Bangombe natural nuclear
814 reaction zones (Franceville basin, Gabon). *Chemical Geology* **171**, 147–171.
815 Melezhik, V. A., Fallick, A. E., Fillippov, M. M., Larsen, O., 1999. Karelian shungite—an
816 indication of 2.0-Ga-old metamorphosed oil-shale and generation of petroleum:
817 geology, lithology and geochemistry. *Earth-Science Reviews* **47**, 1–40.
818 Melezhik, V.A., Huhma, H., Condon, D.J., Fallick, A.E., Whitehouse, M.J., 2007. Temporal
819 constraints on the Paleoproterozoic Lomagundi–Jatuli carbon isotope event. *Geology*
820 **35**, 655–658.
821 Melezhik, V. A., Fallick, A. E., Brasier, A. T., Lepland, A., 2015. Carbonate Deposition in
822 the Palaeoproterozoic Onega Basin from Fennoscandia: A Spotlight on the Transition
823 from the Lomagundi-Jatuli to Shunga Events. *Earth Science Review* **147**, 65–98.
824 Melezhik, V. A., Hanski, E. J., 2012. Palaeotectonic and palaeogeographic evolution of
825 Fennoscandia in the Early Palaeoproterozoic. In: Melezhik, V.A., Prave, A.R.,
826 Hanski, E.J., Fallick, A.E., Lepland, A., Kump, L.R., Strauss, H. (Eds.), The
827 Palaeoproterozoic of Fennoscandia as Context for the Fennoscandian Arctic Russia -
828 Drilling Early Earth Project. Series. *Frontiers in Earth Sciences* **1**, Springer,
829 Heidelberg, pp. 111–178.

Molnár, F., O'Brien, H., Stein, H., Cook, N. D. J., 2017. Geochronology of Hydrothermal Processes Leading to the Formation of the Au–U Mineralization at the Rompas Prospect, Peräpohja Belt, Northern Finland: Application of Paired U–Pb Dating of Uraninite and Re–Os Dating of Molybdenite to the Identification of Multiple Hydrothermal Events in a Metamorphic Terrane. *Minerals* **7**, 171. DOI:10.3390/min7090171.

Mossman, D.J., Nagy, B., Rigali, M.J., Gauthier-Lafaye, F., Holliger, P., 1993. Petrography and paragenesis of organic matter associated with the natural fission reactors at Oklo, Republic of Gabon: a preliminary report. *International Journal of Coal Geology* **24**, 179–194.

Naudet, R., 1991. Oklo: des réacteurs nucléaires fossiles. *Collection du Commissariat à l'Energie Atomique*, Paris, pp. 695.

Negrutsa, V. Z., 1984. Early proterozoic stages of evolution of the eastern Baltic shield. *Nedra*, Leningrad, 270 pp (in Russian).

Negrutsa, V. Z., Polekhovsky, Y. S., 1995. Geodynamic criteria for prospecting and metallogenic evaluation of black shale associations of the Baltic Shield. *Otechestvennaya Geologija* **5**, 50–60 (in Russian).

Neuilly, M., Bussac, J., Frejacques, C., Nief, G., Vendryes, G., Yvon, J., 1972. Sur l'existence dans un passé reculé d'une réaction en chaîne naturelle de fission dans le gisement d'uranium d'Oklo (Gabon). *Comptes Rendus de l'Académie des Sciences Paris* **275**, 1847–1849.

Ojakangas, R. W., Marmo, J. S., Heiskanen, K. I., 2001. Basin evolution of the Paleoproterozoic Karelian Supergroup of the Fennoscandian (Baltic) Shield. *Sedimentary Geology* 141–142, 255–285.

Openshaw, R., Pagel, M., Poty, B., 1978. Phases fluides contemporaines de la diagenèse des grès, des mouvements tectoniques et du fonctionnement des réacteurs nuc1éaires d'Oklo, in: The natural fission reactors. *International Atomic Energy Agency*, Vienna, pp. 267–293.

Ossa Ossa, F., 2010. Etude multi-approches du bassin sédimentaire Paléoprotérozoïque (2.1–2.4 Ga) de Franceville au Gabon: les environnements sédimentaires et l'impact des paléocirculations de fluides. *Ph.D. University of Poitiers, Poitiers, France*, pp. 191.

Ossa Ossa, F. *et al*., 2013. Exceptional preservation of expandable clay minerals in the ca. 2.1 Ga black shales of the Francevillian basin, Gabon and its implication for atmospheric oxygen accumulation. *Chemical Geology* **362**, 181–192.

Ossa Ossa, F., Eickmann, B., Hofmann, A., Planavsky, N.J., Asael, D., Pambo, F., Bekker, A., 2018. Two-step deoxygenation at the end of the Paleoproterozoic Lomagundi Event. *Earth and Planetary Science Letters* **486**, 70–83.

Ossa Ossa, F., Hofmann, A., Ballouard, C., Vorster, C., Schoenberg, R., Fiedrich, A., Mayaga-Mikolo, F., Bekker, A., 2020. Constraining provenance for the uraniferous Paleoproterozoic Francevillian Group sediments (Gabon) with detrital zircon geochronology and geochemistry. *Precambrian Research* **343**, 105724.

Ossa Ossa, F., Hofmann, A., Vidal, O., Kramers, J.D., Agangi, A., Belyanin, G. A., Mayaga-Mikolo, F., 2014. Hydrothermal clay mineral formation in the uraniferous Paleoproterozoic FA Formation, Francevillian basin, Gabon. *Precambrian Research* **246**, 134–149.

Paiste, K. *et al*., 2020a. The pyrite multiple sulfur isotope record of the 1.98 Ga Zaonega Formation: Evidence for biogeochemical sulfur cycling in a semi-restricted basin. *Earth Planet. Sci. Lett.* **534**, 116092. DOI: 10.1016/j.epsl.2020.116092.

878 Paiste, K. *et al*., 2020b. Identifying global vs. basinal controls on Paleoproterozoic organic
879 carbon and sulfur isotope records. *Earth Science Review,* DOI:
880 10.1016/j.earscirev.2020.103230.
881 Pambo, F., Guiraud, M., Quesne, D., Gauthier-Lafaye, F., Azzibrouck, G., Lang, J., 2006.
882 The Proterozoic Franceville Basin (SE Gabon): an example of interaction between
883 marine sedimentation and extensional faulting. *Africa Geoscience Review* **13**, 77–106.
884 Piper, D. Z., Dean, W. E., 2002. Trace-element deposition in the Cariaco Basin, Venezuela
885 shelf, under sulfate-reducing conditions—a history of the local hydrography and
886 global climate, 20 ka to the present. *US Geological Survey*, Professional Paper 1670.
887 DOI: 10.3133/pp1670.
888 Poulton, S. W., Bekker, A., Cumming, V. M., Zerkle, A. L., Canfield, D. E., Johnston, D. T.,
889 2021. A 200 million year delay in permanent atmospheric oxygenation. *Nature* **592**,
890 232–236.
891 Préat, A., Bouton, P., Thiéblemont, D., Prian, J.P., Ndounze, S.S., Delpomdor, F., 2011.
892 Paleoproterozoic high $\delta^{13}C$ dolomites from the Lastoursville and Franceville basins
893 (SE Gabon): stratigraphic and synsedimentary subsidence implications. *Precambrian*
894 *Research* **189**, 212–228.
895 Qu, Y., Črne, A. E., Lepland, A. & Van Zuilen, M. A., 2012. Methanotrophy in a
896 Paleoproterozoic oil field ecosystem, Zaonega Formation, Karelia, Russia.
897 *Geobiology* **10**, 467−478.
898 Qu, Y., Lepland, A., van Zuilen, M. A., Whitehouse, M., Črne, A. E., Fallick, A. E., 2018.
899 Sample-scale carbon isotopic variability and diverse biomass in the Paleoproterozoic
900 Zaonega Formation, Russia. Precambrian Research 315, 222–231.
901 Rudnick, R.L., Gao, S., 2014. Composition of Continental Crust. Eds. Holland, H.D.,
902 Turekian, K.K. *Treatise on Geochemistry* **4**, 1–51.
903 Sadiq, M., 1988. Thermodynamic stability relationships of inorganic vanadium in the marine
904 environment. *Marine Chemistry* **23**, 87–96.
905 Schlesinger, W. H., Klein, E. M., Vengosh, A., 2017. Global biogeochemical cycle of
906 vanadium. *Proceedings of the National Academy of Sciences USA* **114**, E11092–
907 E11100.
908 Scott, C. *et al*., 2014. Pyrite multiple-sulfur isotope evidence for rapid expansion and
909 contraction of the early Paleoproterozoic seawater sulfate reservoir. *Earth and*
910 *Planetary Science Letters* **389**, 95–104.
911 Scott, C., Slack, J. F., Kelley, K. D., 2017. The hyper-enrichment of V and Zn in black shales
912 of the Late Devonian-Early Mississippian Bakken Formation (USA). Chemical
913 Geology 452, 24–33.
914 Skei, J., Loring, D. H., Rantala, R. T. T., 1988. Partitioning and enrichment of trace metals in
915 a sediment core from Framvaren, south Norway. *Marine Chemistry* **23**, 269–281.
916 Thiéblemont, D., Castaing, C., Billa, M., Bouton, P., and Préat, A., 2009. Notice explicative
917 de la carte géologique et des ressources minérales de la République Gabonaise: *Eds*
918 *DGMC – Ministère des Mines, du Pétrole, des Hydrocarbures*, Libreville, pp. 384.
919 Wanty, R. B., Goldhaber, M. B., 1992. Thermodynamics and kinetics of reactions involving
920 vanadium in natural systems: accumulation of vanadium in sedimentary rocks.
921 *Geochimica et Cosmochimica Acta* **56**, 1471–1483.
922 Weber, F., 1968. Une série précambrienne du Gabon: le Francevillien. Sédimentologie,
923 géochimie et relation avec les gîtes minéraux associés. *Mémoire Service Cartes*
924 *Géologique Alsace-Lorraine,* Strasbourg, France, **28**, pp. 328.
925 Weber, F., Gauthier-Lafaye, F., Whitechurch, H., Ulrich, M., El Albani, A., 2016. The 2-Ga
926 Eburnean Orogeny in Gabon and the opening of the Francevillian intracratonic basins:
927 A review. *Comptes Rendus* Geoscience **48**, 572–586.

FIGURE CAPTIONS:

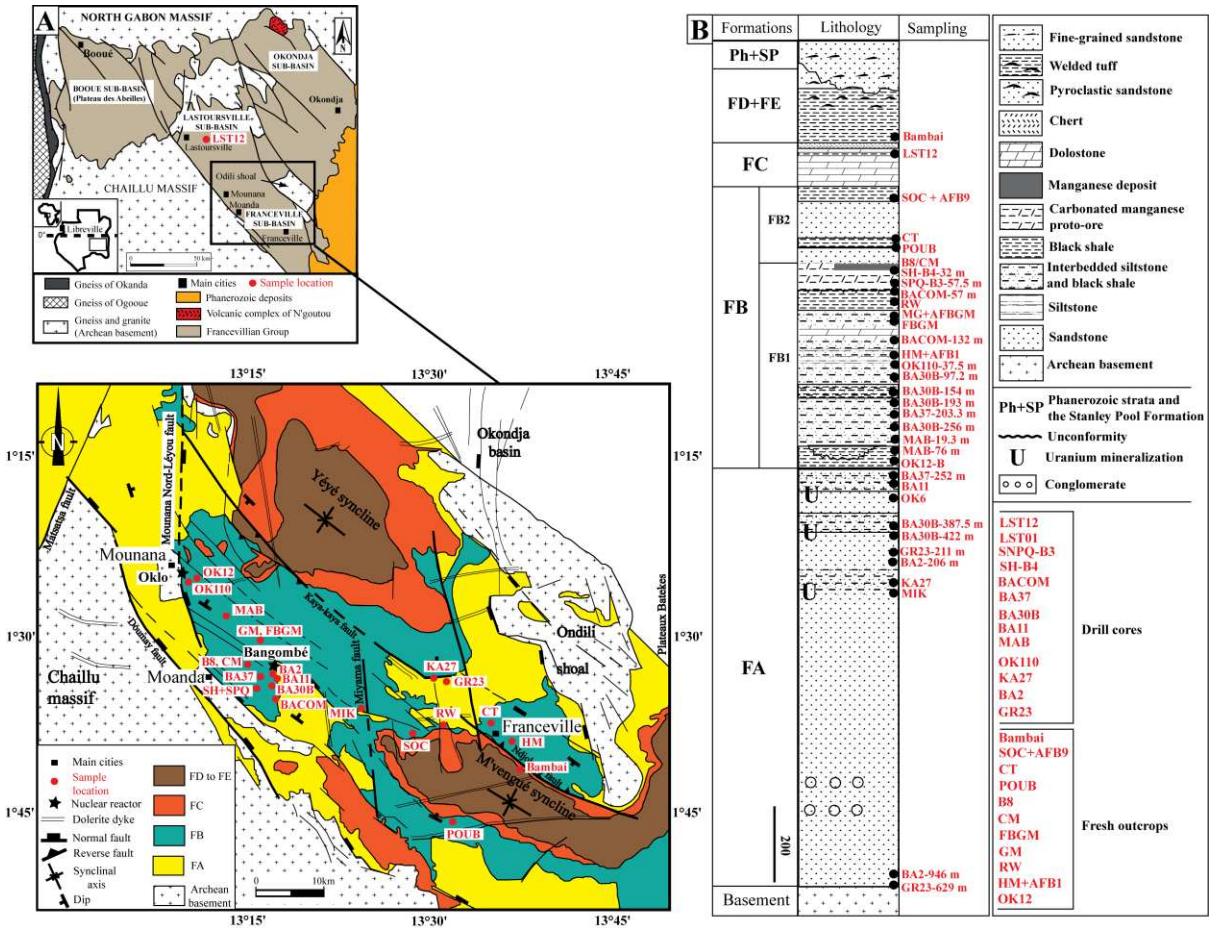

Fig. 1. Geological maps for the Francevillian basin and Franceville sub-basin (**A**) and lithostratigraphic column (**B**) for the Francevillian basin, showing sample locations (modified from Gauthier-Lafaye and Weber, 1989, 2003; Pambo et al., 2006; Weber, 1968).

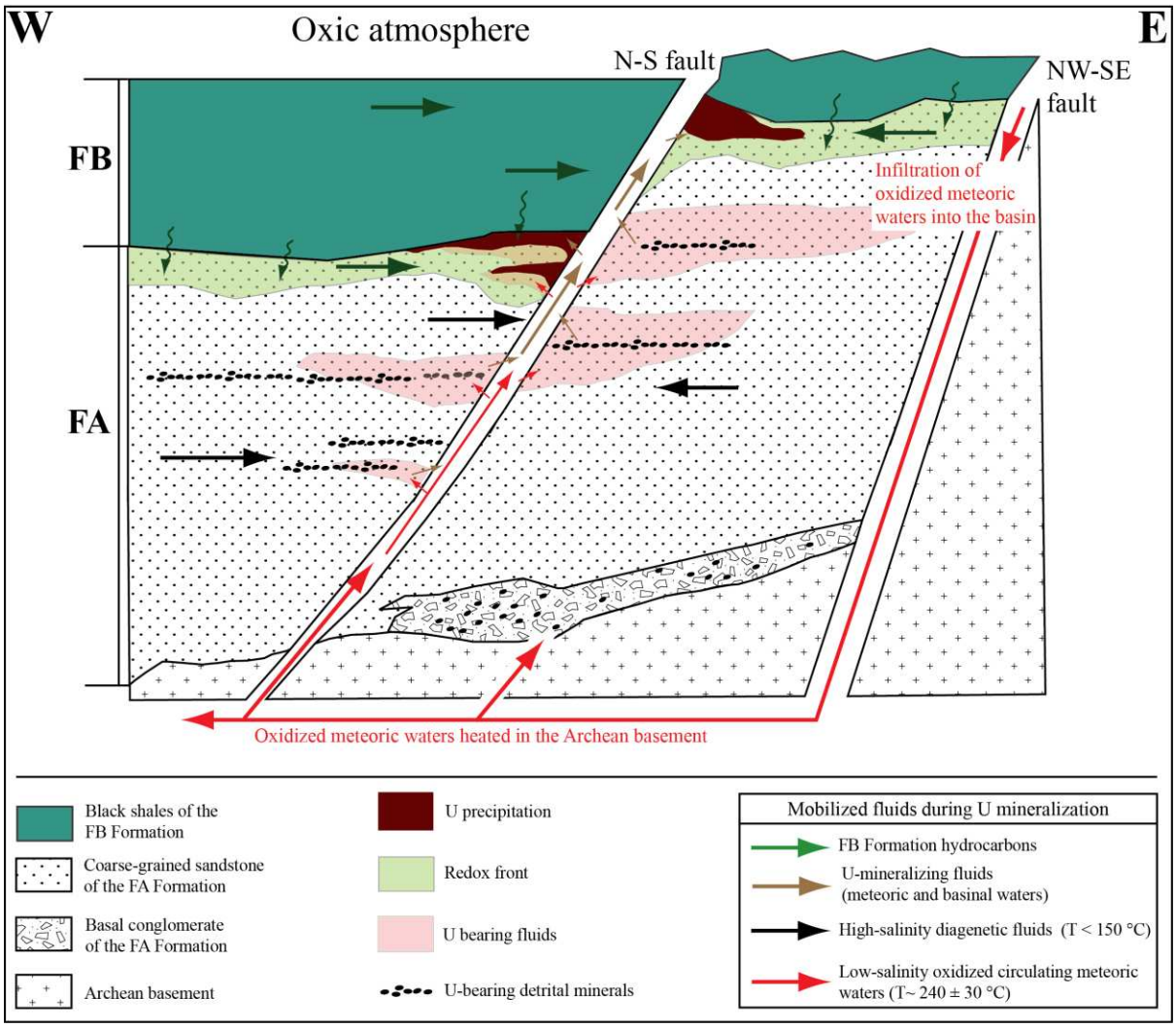

Fig. 2. Francevillian U-ore mineralization model showing different fluid migration paths (modified from Gauthier-Lafaye and Weber, 1989; Mathieu et al., 2000; Ossa Ossa, 2010).

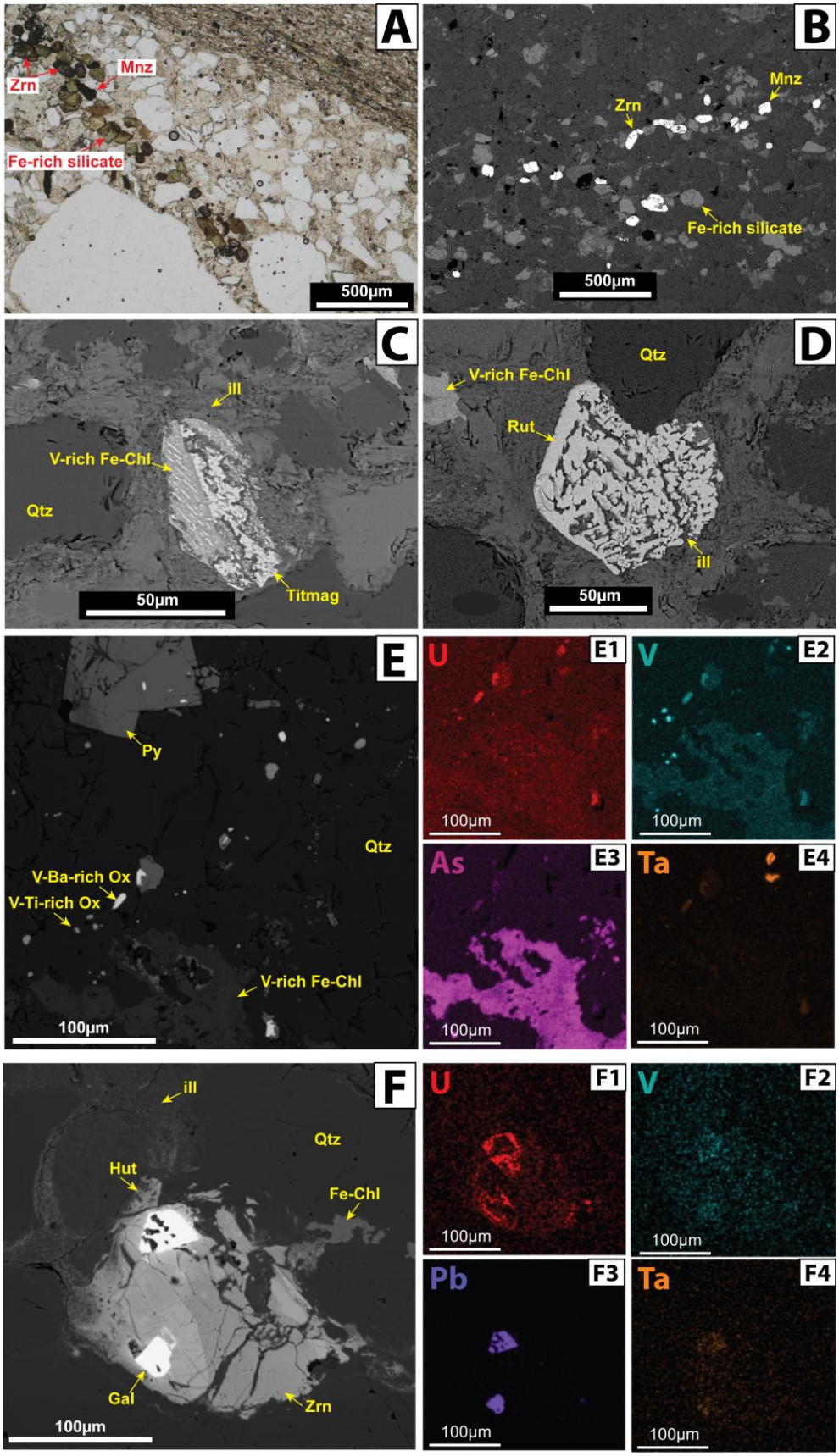

Fig. 3. Petrographic observations for the U-V-bearing sandstone from the FA Formation associated and not associated with natural nuclear reactors. (**A**) Photomicrograph of a sandstone sample close to the Bamgobé natural nuclear reactor showing abundant

heavy detrital minerals, including monazite, zircon and undetermined Fe-rich silicate. (**B**) Backscattered electron (BSE) image of a sandstone sample from the Mikouloungou U-ore deposit (bearing no natural nuclear reactor), confirming an abundance of heavy detrital minerals, including monazite, zircon and Fe-rich silicate. (**C**). BSE image of altered titanomagnetite partially replaced by V-rich Fe-chlorite. (**D**) BSE image of altered rutile partially replaced by illite. (**E**) BSE image from the U-mineralized zone of the Mikouloungou U-ore deposit (bearing no natural nuclear reactor), showing authigenic grains of vanadium oxides together with authigenic V-rich Fe-chlorite. Elemental maps show enrichment of U (**E1**), V (**E2**), As (**E3**) and Ta (**E4**). (**F**) BSE image of altered zircon grain with inclusions of galena. Elemental maps show enrichment in U (**F1**), V (**F2**), Pb (**F3**) and Ta (**F4**). Zrn: zircon; Mnz: monazite; ill: illite; Fe-Chl: iron-rich chlorite; Titmag: titanomagnetite; Rut: rutile; Qtz: quartz; Ox: oxide; Hut: huttonite; Gal: galena.

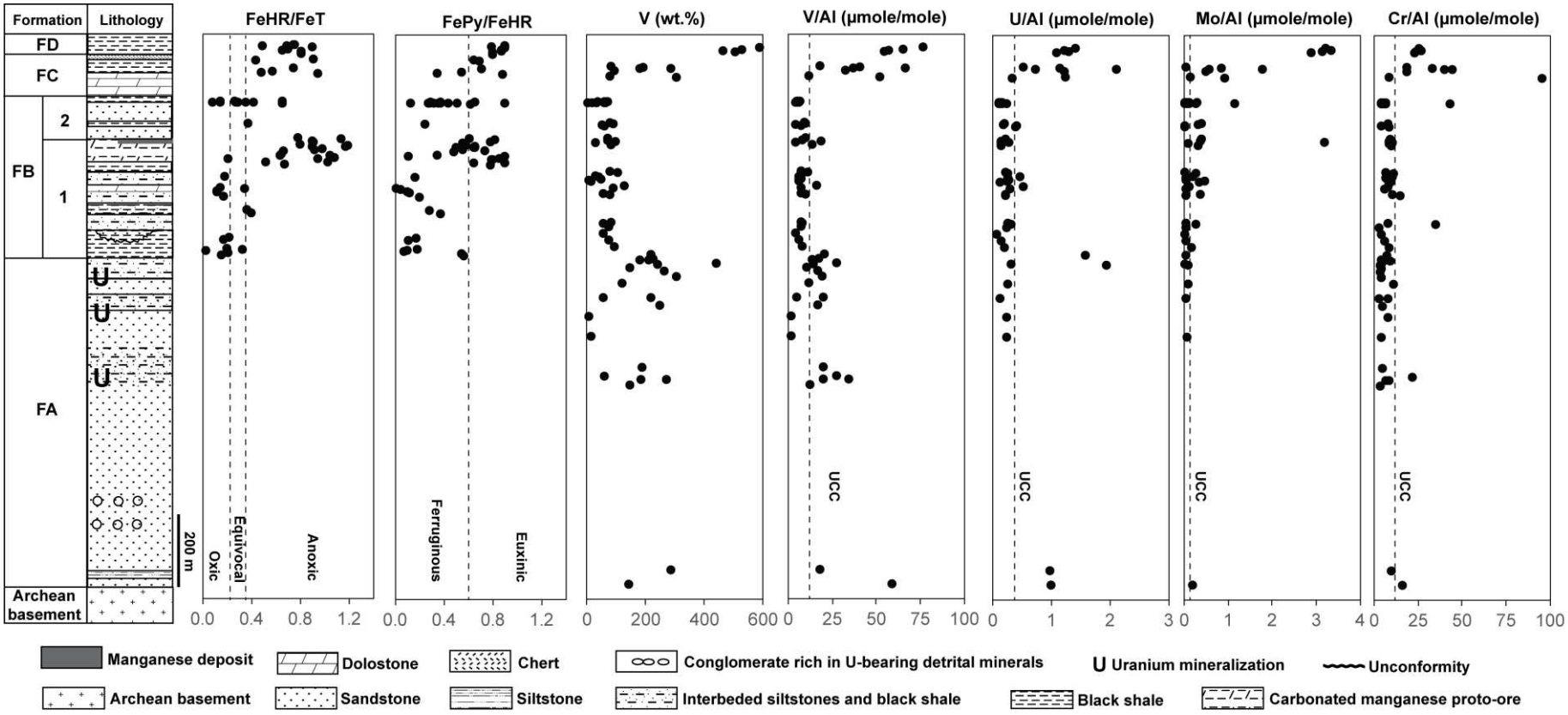

Fig. 4: Lithostratigraphic profile and geochemical data for the Francevillian Group. FeHR/FeT data are from previous studies (Canfield et al., 2013; Ossa Ossa et al., 2018). Oxic, anoxic and equivocal fields of the FeHR/FeT panel as well as euxinic and ferruginous fields of the FePy/FeHR panel are after Poulton and Canfield (2011). Dashed lines on V/Al, U/Al, Mo/Al and Cr/Al plots represent average values for the upper continental crust (UCC; Rudnick and Gao, 2014).

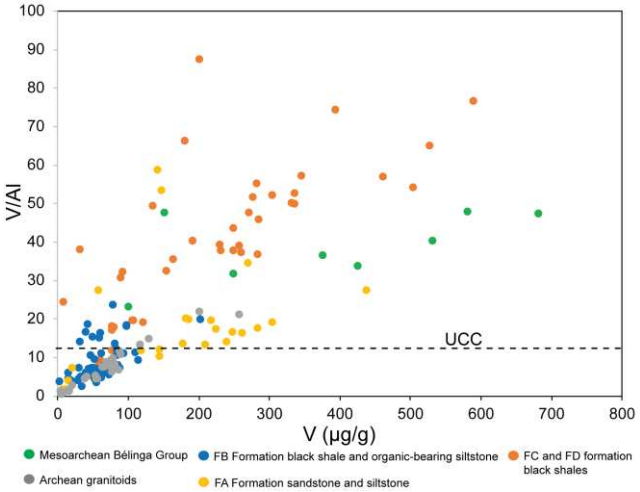

Fig. 5. Cross-plot of V/Al ratios vs. V concentrations, highlighting Mesoarchean mafic to ultramafic igneous rocks of the Bélinga Group in the Archean basement and the FC and FD formation black shales of the Francevillian Group as a potential V source for the FA Formation U-ore deposits. Data are from this study and the literature (Bouton et al., 2009; Thieblement et al., 2009). UCC dashed line represents the average value for the upper continental crust (Rudnick and Gao, 2014).

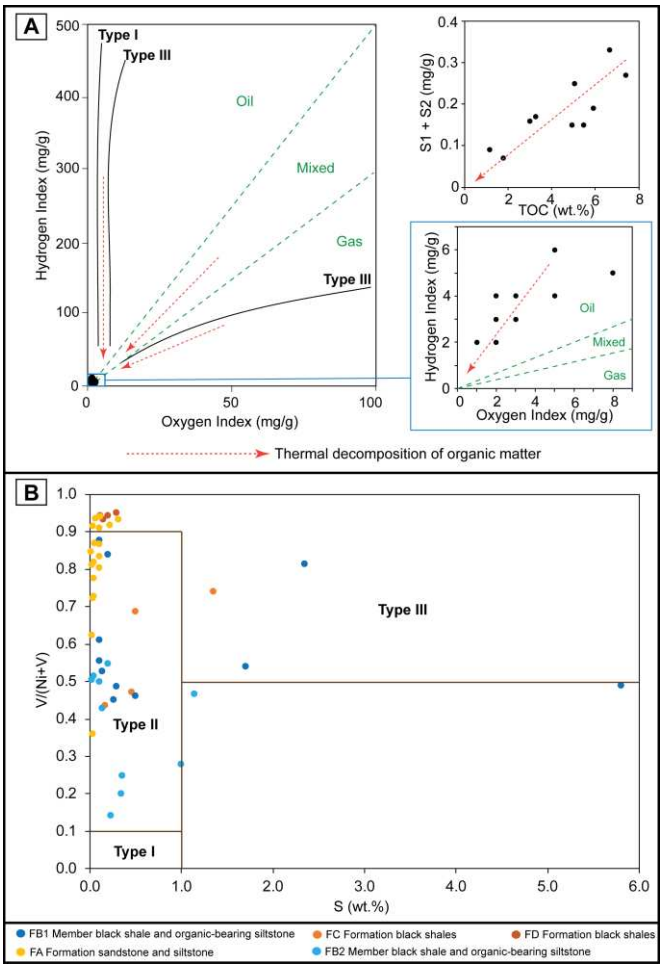

Fig. 6. Petroleum-source rock data for the organic-rich, fine-grained Francevillian sedimentary rocks with (**A**) rock-eval pyrolysis data (after Dembicki, 2009 and reference therein), and (**B**) V/(Ni+V) vs. S (wt.%) cross-plot (after Lewan, 1984; Hatch and Levanthal, 1992).

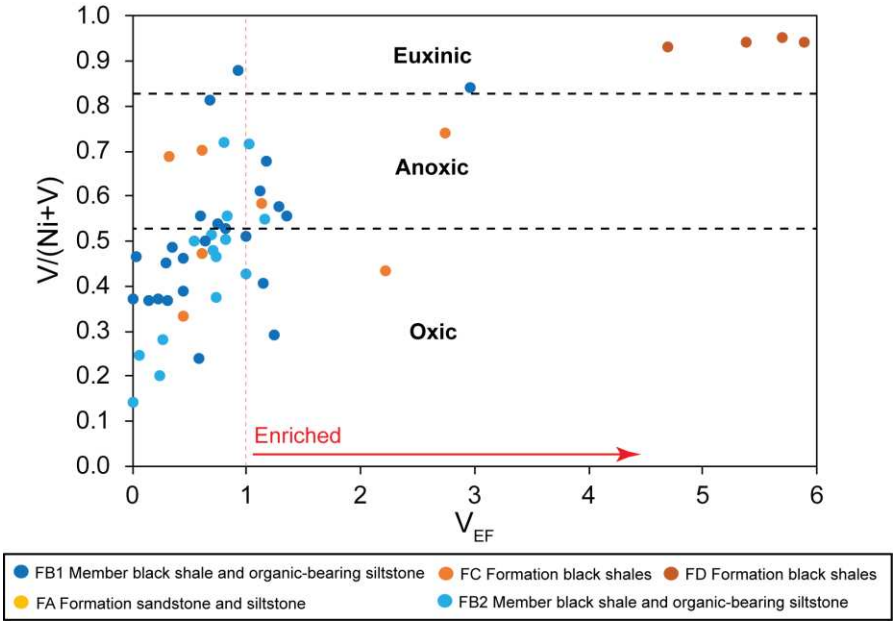

Fig. 7. V/(Ni+V) vs. V enrichment factor (V_{EF}) cross-plot illustrating environmental redox conditions during deposition of the Francevillian Group, organic-rich petroleum-source rocks (after Lewan, 1984; Hatch and Levanthal, 1992). Red dashed line represents the upper continental crust (Rudnick and Gao, 2014).

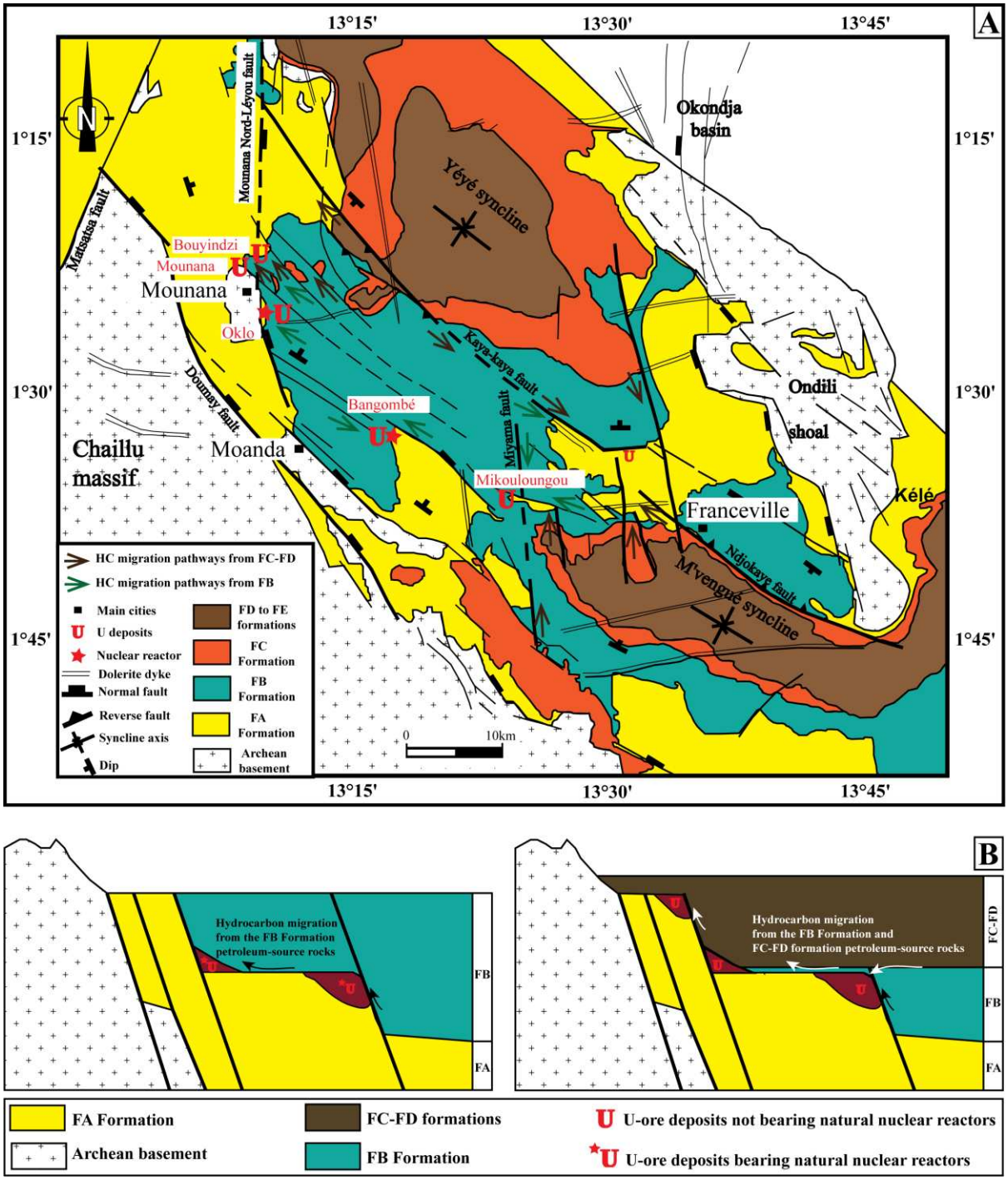

Fig. 8. Geological map of the Franceville sub-basin illustrating hydrocarbon (HC) migration pathways (**A**) and updated model for U-ore mineralization in the Franceville sub-basin showing migration of hydrocarbons derived from the FB and FC-FD formation petroleum-source rocks along regional faults (**B**). Mineralization of V-poor, high-grade U-ore deposits associated with natural nuclear reactors (Oklo-Okelobondo and Bangombé) involved hydrocarbons derived from the FB Formation V-poor petroleum-source rocks. Mineralization of V-rich, high-grade U-ore deposits bearing no natural nuclear reactors (Mounana, Boyindzi and Mikouloungou) involved hydrocarbons derived from the FB Formation V-poor and FC-FD formations V-rich petroleum-source rocks.

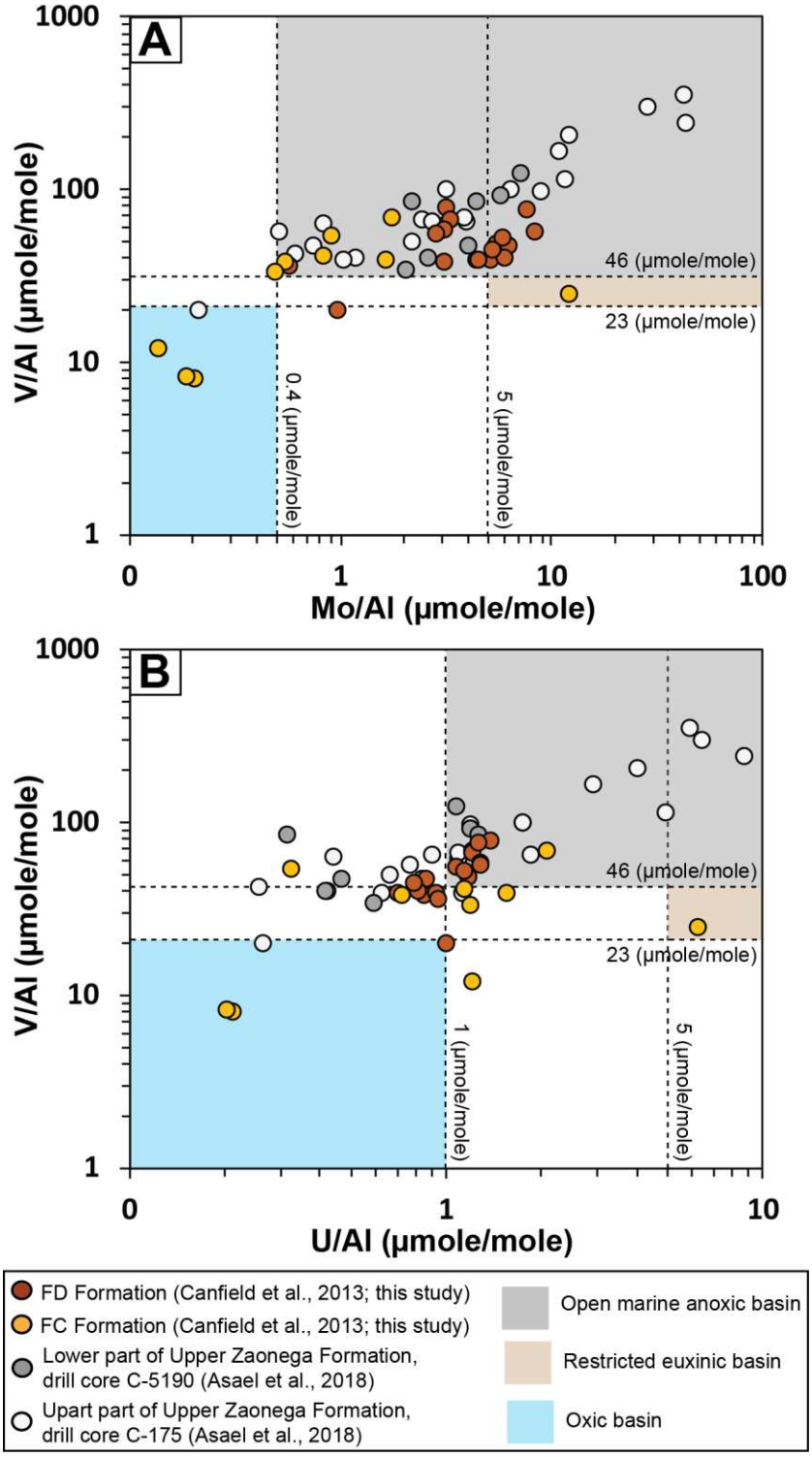

Fig. 9. V/Al vs U/Al and V/Al vs Mo/Al cross-plots (from Bennet and Canfield, 2020) showing the Upper Francevillian Group and Upper Zaonega Formation black shales. The data indicates increasing V, Mo and U enrichments upsection under anoxic, open-marine conditions.

Table 1: Selected major and trace element data for the Francevillian Group

Formation	Sample ID	Litho	Source	Al	Fe	Mn	S	V	Cr	Ni	U	Mo	V/Al	Cr/Al	U/Al	Mo/Al	V/(V+Ni)	V EF	U EF	Cr EF	Mo EF	Ni EF
				%	%	%	%	ppm	ppm	ppm	ppm	ppm										
FD	**Bambai 5 a**	BS	Outcrop	7.7	1.1	0.0	0.3	588.0	193.7	29.7	10.8	24.7	76.7	25.3	1.4	3.2	1.0	6.44	4.25	2.24	23.87	0.67
	Bambai 5 b	BS	Outcrop	8.1	0.5	0.0	0.1	526.0	214.6	31.8	9.9	27.1	65.0	26.5	1.2	3.3	0.9	5.46	3.69	2.35	24.82	0.68
	Bambai 5 c	BS	Outcrop	8.1	0.6	0.0	0.1	460.0	193.2	33.0	10.5	25.4	57.1	24.0	1.3	3.2	0.9	4.79	3.93	2.12	23.34	0.71
	Bambai 5 d	BS	Outcrop	9.3	0.5	0.0	0.2	503.0	212.0	30.0	10.1	26.8	54.4	22.9	1.1	2.9	0.9	4.57	3.30	2.03	21.46	0.56
FC	**LST12-24.7m**	BS	Drill core	4.4	2.1	0.3		79.0	83.3	157.3	2.3	0.2	18.0	18.9	0.5	0.0	0.3	1.51	1.58	1.68	0.34	6.20
	LST12-26.05m	BS	Drill core	4.7	3.5	0.1		190.3	156.2	136.4	5.4	4.0	40.5	33.2	1.1	0.9	0.6	3.40	3.47	2.94	6.31	5.03
	LST12-31.3m	BS	Drill core	2.7	7.7	2.8		179.5	107.3	76.5	5.7	4.8	66.5	39.7	2.1	1.8	0.7	5.59	6.37	3.52	13.17	4.91
	LST 12-32m	BS	Drill core	7.7	2.7	7.5	1.4	282.0	342.0	98.0	5.6	4.3	36.7	44.6	0.7	0.6	0.7	3.09	2.20	3.95	4.15	2.21
	LST12-36.05m	BS	Drill core	2.8	1.6	0.1	0.5	90.8	52.3	41.1	3.4	1.4	32.4	18.7	1.2	0.5	0.7	2.72	3.67	1.65	3.70	2.55
	LST12-57.05m	BS	Drill core	6.4	1.9	0.1	0.5	75.7	55.4	84.3	7.9	0.9	11.8	8.7	1.2	0.1	0.5	0.99	3.73	0.77	1.04	2.28
	LST12-59.7m	BS	Drill core	5.8	5.1	0.1	0.2	303.3	553.1	391.8	1.9	5.3	52.3	95.4	0.3	0.9	0.4	4.39	0.99	8.45	6.77	11.71
FB2	**AFB9-18**	BS	Outcrop	9.9	2.4	0.1	1.1	66.9	54.8	53.2	1.2	0.8	6.8	5.5	0.1	0.1	0.6	0.57	0.37	0.49	0.57	0.93
	SOC-A2	BS	Outcrop	13.9	1.8	0.6	0.2	66.3	57.7	54.5	1.5	0.3	4.8	4.1	0.1	0.0	0.5	0.40	0.33	0.37	0.16	0.68
	SOC-B	BS	Outcrop	13.4	1.8	0.3	0.1	59.2	55.5	79.1	1.4	1.0	4.4	4.1	0.1	0.1	0.4	0.37	0.32	0.37	0.55	1.02
	SOC-C	BS	Outcrop	9.5	2.1	0.2	0.0	58.1	54.3	54.5	1.4	0.2	6.1	5.7	0.1	0.0	0.5	0.51	0.44	0.51	0.16	0.99
	SOC-105	BS	Outcrop	10.1	2.9	0.4		57.9	60.5	66.6	1.3	0.6	5.7	6.0	0.1	0.1	0.5	0.48	0.39	0.53	0.44	1.14
	SOC-112	BS	Outcrop	10.0	3.6	0.4		56.4	64.7	61.0	1.4	0.3	5.6	6.5	0.1	0.0	0.5	0.47	0.42	0.57	0.22	1.06
	SOC-111	BS	Outcrop	10.0	2.8	0.3		57.9	53.5	96.5	1.3	2.8	5.8	5.3	0.1	0.3	0.4	0.49	0.39	0.47	2.07	1.67
	AFB9-07	BS	Outcrop	6.4	4.5	0.6	1.0	32.4	40.6	83.2	1.1	0.8	5.1	6.4	0.2	0.1	0.3	0.43	0.51	0.56	0.88	2.26
	AFB9-02	BS	Outcrop	6.4	6.2	0.1	0.3	29.1	30.2	115.1	1.0	0.7	4.6	4.7	0.2	0.1	0.2	0.38	0.48	0.42	0.84	3.13
	AFB9-HG	BS	Outcrop	3.1	5.0	2.5	0.4	14.2	21.1	43.2	0.7	0.8	4.6	6.8	0.2	0.3	0.2	0.39	0.72	0.60	1.91	2.41
	AFB9-4	BS	Outcrop	0.5	0.1	0.0	0.2	1.9	21.6	11.6	0.1	0.6	3.9	43.2	0.2	1.2	0.1	0.32	0.74	3.83	8.52	4.04

	CT-004	BS	Outcrop	8.3	0.8	0.1		76.2	64.4	29.8	1.7	3.3	9.2	7.7	0.2	0.4	0.7	0.77	0.62	0.69	2.94	0.62
	CT-001	BS	Outcrop	9.2	0.7	0.1		87.7	70.5	34.6	1.6	2.9	9.5	7.6	0.2	0.3	0.7	0.80	0.52	0.68	2.33	0.65
	POUB. B	BS	Outcrop	7.7	1.2	0.0	0.1	55.4	64.0	55.3	3.0	0.1	7.2	8.3	0.4	0.0	0.5	0.60	1.18	0.74	0.10	1.25
	POUB. E	BS	Outcrop	12.8	1.4	0.0	0.0	50.9	54.5	49.8	5.2	0.2	4.0	4.3	0.4	0.0	0.5	0.33	1.23	0.38	0.12	0.67
	B8-CM2	BS	Outcrop	7.0	4.6	6.3	5.8	66.9	65.1	53.4	1.5	2.8	9.5	9.3	0.2	0.4	0.6	0.80	0.65	0.82	2.96	1.32
	B8-04	BS	Outcrop	8.1	1.8	0.0	2.3	66.5	68.3	15.1	1.1	3.0	8.2	8.4	0.1	0.4	0.8	0.69	0.41	0.75	2.74	0.32
	SH2-B4-32m	BS	Drill core	5.2	3.8	0.1		95.8	55.8	95.6	1.4	16.7	18.3	10.7	0.3	3.2	0.5	1.54	0.80	0.94	23.67	3.17
	BACOM-57m	BS	Drill core	5.8	2.1	5.4		80.0	55.2	254.0	0.8	1.8	13.8	9.5	0.1	0.3	0.2	1.16	0.41	0.84	2.33	7.58
	SPQ1-B3-57.9m	BS	Drill core	6.6	1.8	0.0		27.6	55.4	46.4	1.0	0.6	4.2	8.4	0.2	0.1	0.4	0.35	0.46	0.74	0.72	1.22
	RW-106	BS	Outcrop	10.5	5.2	0.1		74.4	68.4	71.0	2.2	0.2	7.1	6.5	0.2	0.0	0.5	0.59	0.63	0.58	0.14	1.17
	RW-105	BS	Outcrop	9.3	8.9	0.1		100.6	103.8	47.4	2.3	2.5	10.8	11.2	0.2	0.3	0.7	0.91	0.75	0.99	2.00	0.89
	BACOM-132m	BS	Drill core	2.0	0.5	0.7		11.3	17.7	13.0	0.2	0.7	5.8	9.0	0.1	0.3	0.5	0.48	0.35	0.80	2.57	1.15
	AFB1-03	BS	Outcrop	11.8	1.0	0.0		86.2	72.7	63.0	3.5	0.6	7.3	6.2	0.3	0.0	0.6	0.62	0.89	0.55	0.36	0.93
	FBGM-09	BS	Outcrop	3.9	1.2	0.0		28.3	39.9	48.7	1.8	0.8	7.3	10.2	0.5	0.2	0.4	0.61	1.42	0.91	1.44	2.17
FB1	**AFBGM-08**	BS	Outcrop	6.3	3.1	0.3		39.2	55.9	66.8	1.6	0.5	6.2	8.8	0.3	0.1	0.4	0.52	0.76	0.78	0.57	1.82
	AFBGM-01	BS	Outcrop	0.8	1.1	0.2		5.1	6.9	8.5	0.2	0.4	6.1	8.3	0.2	0.5	0.4	0.52	0.73	0.74	3.43	1.79
	BA30B-193m	BS	Drill core	11.3	1.8	0.0		79.8	90.6	116.0	2.9	0.4	7.0	8.0	0.3	0.0	0.4	0.59	0.77	0.71	0.28	1.77
	MG4	BS	Outcrop	6.2	2.0	0.3	0.3	38.5	40.3	46.5	1.6	0.2	6.2	6.5	0.3	0.0	0.5	0.52	0.78	0.58	0.24	1.30
	FBGM-S-4	BS	Outcrop	6.2	3.6	0.3	0.3	45.5	50.5	47.8	1.7	0.2	7.4	8.2	0.3	0.0	0.5	0.62	0.83	0.72	0.24	1.34
	HM-003	BS	Outcrop	7.7	0.8	0.1		126.8	59.4	305.6	4.0	0.8	16.4	7.7	0.5	0.1	0.3	1.38	1.56	0.68	0.77	6.84
	OK110-37.25m	BS	Drill core	7.9	4.1	0.3	1.7	75.2	118.6	64.2	1.7	0.4	9.5	15.0	0.2	0.1	0.5	0.80	0.65	1.33	0.37	1.41
	BA30B-97.2m	BS	Drill core	7.0	2.1	0.1	0.5	51.3	72.3	59.6	1.5	2.5	7.4	10.4	0.2	0.4	0.5	0.62	0.65	0.92	2.66	1.48
	BA37-203.3m	BS	Drill core	10.1	1.8	0.0	0.1	72.8	30.7	10.1	2.4	0.4	7.2	3.0	0.2	0.0	0.9	0.61	0.72	0.27	0.29	0.17
	BA30B-192.8m	BS	Drill core	6.6	2.5	0.2		53.7	230.8	84.3	2.1	1.7	8.2	35.2	0.3	0.3	0.4	0.69	0.97	3.12	1.92	2.23

	BA30B-256m	BS	Drill core	12.2	1.8	0.0	0.1	72.1	74.4	45.7	1.7	0.4	5.9	6.1	0.1	0.0	0.6	0.49	0.42	0.54	0.24	0.65
	MAB-19.3m	BS	Drill core	12.4	4.0	0.0	0.1	52.2	49.9	46.8	0.8	0.3	4.2	4.0	0.1	0.0	0.5	0.35	0.20	0.36	0.18	0.66
	MAB-76m	BS	Drill core	11.7	2.9	0.0	0.1	91.9	100.3	73.4	2.3	1.8	7.9	8.6	0.2	0.2	0.6	0.66	0.59	0.76	1.14	1.09
	OK12B	BS	Outcrop	10.8	0.3	0.0	0.2	217.4	78.0	41.2	17.0	0.4	20.2	7.2	1.6	0.0	0.8	1.70	4.77	0.64	0.28	0.66
	BA37-221.1m*	BS	Drill core	12.8	6.1	0.1	0.1	223.0	55.0	44.0	-	-	17.5	4.3	-	-	0.8	1.47	-	0.38	-	0.60
	BA37-252.4m*	BS	Drill core	15.6	1.8	0.0	0.1	208.0	145.0	32.0	-	-	13.3	9.3	-	-	0.9	1.12	-	0.82	-	0.36
	BA11-49m*	BS	Drill core	12.9	4.1	0.0	0.0	176.0	69.0	39.0	-	-	13.7	5.4	-	-	0.8	1.15	-	0.47	-	0.53
	BA11-74m*	BS	Drill core	13.9	4.4	0.0	0.0	143.0	60.0	55.0	-	-	10.3	4.3	-	-	0.7	0.87	-	0.38	-	0.69
	BA11-176.9m*	BS	Drill core	15.7	3.2	0.0	0.1	303.0	64.0	45.0	-	-	19.3	4.1	-	-	0.9	1.62	-	0.36	-	0.50
	BA11-200.06m*	BS	Drill core	14.9	5.3	0.0	0.0	247.0	75.0	71.0	-	-	16.6	5.0	-	-	0.8	1.39	-	0.45	-	0.83
	KA27-99.2m**	BS	Drill core	15.9	4.4	0.0	0.1	437.1	67.6	42.5	4.9	0.2	27.5	4.3	0.3	0.0	0.9	2.31	0.93	0.38	0.09	0.46
	KA27-114.75m	BS	Drill core	16.8	1.8	0.0	0.2	238.0	56.7	21.1	32.7	1.4	14.2	3.4	1.9	0.1	0.9	1.19	5.88	0.30	0.62	0.22
FA	**KA27-137.4m****	BS	Drill core	15.8	2.1	0.0	0.1	261.0	60.0	18.0	-	-	16.5	3.8	-	-	0.9	1.39	-	0.34	-	0.20
	GR23-211.5m**	SST	Drill core	9.3	1.5	0.0	0.0	185.0	45.0	17.0	-	-	20.0	4.9	-	-	0.9	1.68	-	0.43	-	0.32
	OK 6*	ST	Outcrop	2.0	0.2	0.0	0.0	56.0	45.0	21.0	-	-	27.5	22.1	-	-	0.7	2.31	-	1.96	-	1.79
	BA30B-387.5m*	SST	Drill core	9.9	2.2	0.0		117.4	110.2	24.9	2.5	0.9	11.9	11.2	0.3	0.1	0.8	1.00	0.76	0.99	0.68	0.44
	BA30B-422.23m*	SST	Drill core	11.0	2.6	0.0	0.0	217.0	87.0	39.0	-	-	19.8	7.9	-	-	0.8	1.66	-	0.70	-	0.62
	Mik 5 **	BS	Outcrop	11.8	1.0	0.0	0.1	144.0	42.0	35.0	-	-	12.2	3.6	-	-	0.8	1.03	-	0.32	-	0.52
	Mik 1**	ST	Outcrop	7.8	1.3	0.0	0.1	269.0	68.0	17.0	-	-	34.5	8.7	-	-	0.9	2.90	-	0.77	-	0.38
	Mik 1B**	ST	Outcrop	8.9	0.8	0.0	0.3	180.0	59.0	13.0	-	-	20.2	6.6	-	-	0.9	1.70	-	0.59	-	0.25
	BA30B-422m*	GS	Drill core	11.8	3.3	0.0	0.0	53.4	33.8	32.2	1.5	0.5	4.5	2.9	0.1	0.0	0.6	0.38	0.38	0.25	0.29	0.47
	BA2-206m*	SST	Drill core	2.9	1.1	0.1		4.9	22.9	20.9	0.7	0.0	1.7	8.0	0.2	-	0.2	0.14	0.72	0.71	0.0	1.26

GR23-207m**	GS	Drill core	5.5	1.0	0.0	0.0	10.5	23.3	18.5	1.3	0.4	1.9	4.3	0.2	0.1	0.4	0.16	0.72	0.38	0.54	0.59
BA2-946m*	SST	Drill core	15.9	3.0	0.0	0.0	281.9	153.1	65.8	15.3	0.0	17.8	9.6	1.0	-	0.8	1.49	2.92	0.85	0.0	0.72
GR23-629m**	ST	Drill core	2.4	0.5	0.0		140.1	39.1	13.9	2.4	0.4	58.7	16.4	1.0	0.2	0.9	4.93	2.97	1.45	1.38	1.01

EF: enrichment factor calculated as ($element_{sample}/Al_{sample}$)/($element_{UCC}/Al_{UCC}$); UCC: upper continental crust concentration from Rudnick and Gao (2014), with Al_{UCC} = 8.15 %; V_{UCC} = 97 ppm; U_{UCC} = 2.7 ppm; Cr_{UCC} = 92 ppm; Mo_{UCC} = 1.1 ppm; Ni_{UCC} = 47 ppm; -: not measured; *: samples from FA Formation areas with natural nuclear reactors; **: samples from FA Formation areas without natural nuclear reactors; Numbers next to drill core samples represent the depth of samples in meters (m); Litho = lithology; ST = sandstone; SST = siltstone; GS = green shale; BS = black shale.